JCI The Journal of Clinical Investigation

Graft-versus-host disease reduces lymph node display of tissue-restricted self-antigens and promotes autoimmunity

Simone Dertschnig, … , Clare L. Bennett, Ronjon Chakraverty

J Clin Invest. 2020. https://doi.org/10.1172/JCI133102.

Research In-Press Preview Autoimmunity Transplantation

Graphical abstract

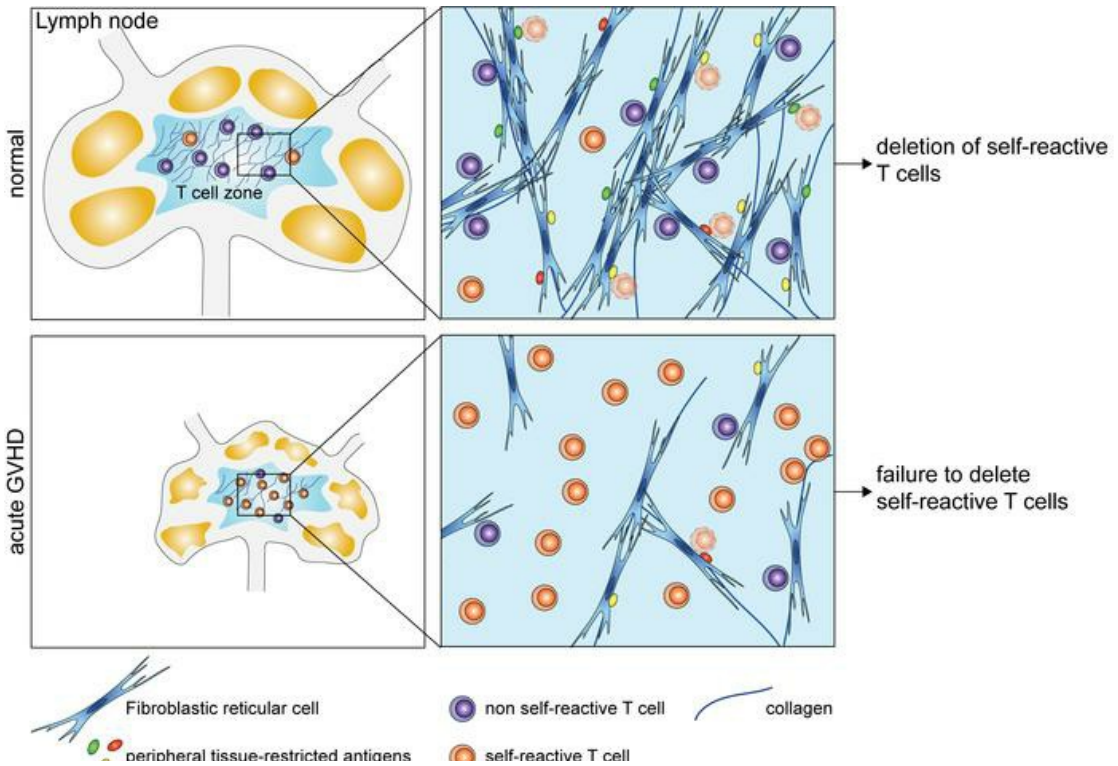

Graft-versus-host disease reduces lymph node display of tissue-restricted self-antigens and promotes autoimmunity

Simone Dertschnig[1,2,*], Pamela Evans[1,2,*], Pedro Santos e Sousa[1,2], Teresa Manzo[3], Ivana R. Ferrer[1,2], Hans J. Stauss[2], Clare L. Bennett[1,2] and Ronjon Chakraverty[1,2]

[1]UCL Cancer Institute, [2]Institute of Immunity and Transplantation, London UK and [3]European Institute of Oncology, Milan, Italy

*Contributed equally

Short title: Loss of peripheral tolerance in GVHD

Corresponding author:

Professor Ronjon Chakraverty
Professor of Haematology and Cellular Immunotherapy,
Cancer Institute and Institute of Immunity & Transplantation,
Royal Free Campus, Rowland Hill Street,
London, NW3 2PF, UK

Tel: +44 207 794 0500 ext. 22474
Fax: +44 0207 830 2092
e-mail: r.chakraverty@ucl.ac.uk

Abstract

Acute graft-versus-host disease (GVHD) is initially triggered by alloreactive T cells, which damage peripheral tissues and lymphoid organs. Subsequent transition to chronic GVHD involves the emergence of autoimmunity although the underlying mechanisms driving this process are unclear. Here, we tested the hypothesis that acute GVHD blocks peripheral tolerance of autoreactive T cells by impairing lymph node (LN) display of peripheral tissue-restricted antigens (PTA). At the initiation of GVHD, LN fibroblastic reticular cells (FRC) rapidly reduced expression of genes regulated by DEAF1, an Autoimmune Regulator-like transcription factor required for intra-nodal expression of PTA. Subsequently, GVHD led to the selective elimination of the FRC population, and blocked the repair pathways required for its regeneration. We used a transgenic mouse model to show that the loss of presentation of an intestinal PTA by FRC during GVHD resulted in the activation of auto-aggressive T cells and gut injury. Finally, we show that FRC normally expressed a unique PTA gene signature that was highly enriched for genes expressed in the target organs affected by chronic GVHD. In conclusion, acute GVHD damages and prevents repair of the FRC network, thus disabling an essential platform for purging auto-reactive T cells from the repertoire.

Introduction

The success of allogeneic hematopoietic stem cell transplantation is limited by the occurrence of graft-versus-host disease (GVHD), an acute inflammatory process triggered by the influx of alloreactive effector T cells into barrier surface tissues (primarily skin and gut) and lymphoid organs (1). Although acute GVHD may resolve with corticosteroid treatment, its occurrence is a strong predictor for the later development of chronic GVHD; in this case, organ involvement is often more extensive than the acute disease and clinical features include many features reminiscent of classic autoimmune disorders (e.g. scleroderma, sicca syndrome and immune cytopenias) (2).

The mechanisms underpinning the transition from acute to chronic GVHD are poorly understood. Donor T cells with autoreactivity can readily be detected 2-5 weeks after the onset of acute GVHD in mice (3-6); autoreactivity is inferred because these T cells can induce widespread tissue injury upon secondary transfer to recipient mice *syngeneic* to the donor and do so with patterns that re-capitulate those observed in chronic GVHD (4, 6, 7). Acute GVHD also targets the thymus and disrupts central tolerance, the process by which T cells reactive against self-antigens are eliminated from the repertoire (5, 8-11). Medullary thymic epithelial cells (mTEC) are particularly sensitive to immune injury in GVHD (9); these stromal cells display peripheral tissue-restricted antigens (PTAs) through a process that requires the transcription factor, Autoimmune Regulator (AIRE) and are normally required for the negative selection of self-reactive thymocytes (12). Loss of mTECs in mice with acute GVHD therefore allows escape of autoreactive T cells into the periphery (8). A 'two-hit' hypothesis for the development of chronic GVHD has been proposed that invokes this loss of central tolerance ('hit one') and a second insult to peripheral tolerance mechanisms ('hit two'), creating conditions favouring unchecked T cell autoreactivity and inflammation (8, 13). A better understanding of how such peripheral regulatory mechanisms fail in GVHD will be critical to preventing the emergence of autoimmunity and chronic tissue injury.

Similar to mTEC, lymph node (LN) non-hematopoietic stromal cells directly present PTA and also trigger deletion of self-reactive T cells (14-17). Peripheral PTA display may exist to reinforce tolerance of autoreactive T cells escaping thymic negative selection or alternatively, provide a means of purging the repertoire of T cells directed to self-antigens not expressed by mTEC. Individual LN stromal populations express distinct repertoires of PTA regulated by mechanisms that are AIRE-independent, for example involving the AIRE-like transcription factor, deformed epidermal autoregulatory factor 1 homologue (DEAF1) (14, 18). The fibroblastic reticular cell (FRC) population is a subset of LN stromal cells lacking hematopoietic (CD45) and endothelial (CD31) markers but expressing a small membrane glycoprotein, podoplanin (or gp38), and the constitutive chemokine CCL19; they form a physical scaffold within the T cell zone and are particularly well positioned to present PTA to naïve T cells in the steady state (19).

In contrast to their inhibitory functions in regulating T cell autoreactivity to PTA, FRC have recently been shown to initiate T cell reactivity to alloantigens in GVHD (20). This role in priming depends upon up-regulated expression of Notch ligands by FRC and may explain the subsequent targeting of this population by the ensuing alloreactive T cell response, leading eventually to severe disruption of the FRC network in several models of GVHD (21). Damage to the FRC network and overall LN structure in murine GVHD mirrors the damage to the T cell zones of lymph nodes described in human patients following transplant (22, 23). FRC targeting in GVHD correlates with profound defects in T–cell dependent antibody immunity (21), a finding consistent with known functions of FRC in promoting cell interactions and LN remodelling to accommodate rapidly expanding immune populations (24, 25).

FRC network injury can also occur following viral infection (e.g. acute lymphocytic choriomeningits, LCMV) but is followed by rapid restoration upon clearance of infection (26). Repair of the FRC network following LCMV infection triggers a lymphoid organ transcriptional ‘re-organisation programme’ involving increased expression of several genes (e.g. *Vcam1, Icam1, Cxcl13, Ltbr*) that are essential for the formation of LN in the embryo and critical for the crosstalk between

lymphoid tissue organiser (LTo) cells (putative precursors to the FRC population) and lymphoid tissue inducer (LTi) cells that express an isoform of RAR-related orphan receptor gamma (RORγt). Scandella and colleagues have proposed that FRC injury in acute LCMV infection in adults recapitulates the embryonic process, where emergence of a reorganizational transcriptional signature is accompanied by rapid LN accumulation of RORγt$^+$ LTi cells (26). Lack of RORγt$^+$ LTi-like cells at the time of acute LCMV infection was shown to impair FRC network restoration (26). Whether such a repair process is operative in the context of FRC injury in GVHD is not known.

Although disruption to the FRC network of LN may help to explain the characteristic immune deficiency of GVHD, its impact upon peripheral tolerance has not been examined. Here, we tested the hypothesis that degeneration of LN stroma during acute GVHD disrupts their role in the peripheral education of self-reactive T cells. We find that the FRC network fails to regenerate following the onset of acute GVHD even when the initial immune response is curtailed. As a consequence of early PTA gene down-regulation and subsequent loss of the FRC network, the normal process of purging of auto-aggressive CD8$^+$ T cells from the peripheral repertoire does not occur. Finally, we show that steady state FRC express a distinct PTA gene signature that is highly enriched for genes normally expressed in target organs affected by chronic GVHD. Thus, repair of stromal populations in lymphoid organs and restoration of PTA display may be essential to prevent the transition from acute to chronic GVHD.

Results

Acute transcriptional response of FRC to GVHD

To permit rapid remodelling of the LN, FRC show exquisite sensitivity to a broad spectrum of pro-inflammatory stimuli, modulating expression of genes with functions relating to the cell cycle and survival (27-29). To determine the acute transcriptional response of FRC to inflammation induced by GVHD, we performed RNAseq analysis of FRC cells (identified as a $CD45^{-}gp38^{+}CD31^{-}$ population) isolated from mice with and without GVHD on day 7. In these experiments, GVHD was induced following an MHC-matched (B6, H-2^{b}), female→male (F→M) bone marrow transplantation (BMT) by co-transfer of T-cell depleted bone marrow (TCDBM) and $CD8^{+}$ MataHari (Mh) T cells transgenic for a T cell receptor (TCR) reactive with male antigen (30). Compared with no GVHD controls (TCDBM), FRC isolated from GVHD mice (TCDBM+T) showed increased representation of gene ontology (GO) terms for cell cycle, apoptosis, NF-κB activation and DNA repair. In contrast, we observed reduced representation of GO terms associated with cell morphogenesis, including those relating to formation of branching structures and vascularisation (Figure 1A). Although there were some differences (for example, increased expression of pathways relating to NF-κB activation in acute GVHD), we observed remarkably similar changes in gene expression in FRC early following herpes simplex virus (HSV) infection (27) suggesting that components of the transcriptional response represent default programs triggered by inflammation (Supplementary Figure 1). However, in sharp contrast to other inflammatory conditions where FRC population expansion is induced (27-29), we observed (using RT-PCR) early down-regulation of genes encoding *Il7* and *Ccl19*, genes that are critical for FRC functions in supporting the survival and homing of naïve T cells (19) (Figure 1B). We also sought to determine how the acute transcriptional response to GVHD would affect PTA gene expression in FRC. We first examined expression of genes encoding AIRE and DEAF1, transcriptional regulators of PTA expression in the thymus (31) and LN (18) respectively. Consistent with published data (15), *Aire* gene expression was not detectable in FRC under any condition (data not shown). *Deaf1* was expressed in control FRC as described previously (15), but its expression was significantly

reduced in the presence of acute GVHD (Figure 1C). To determine if expression levels of genes regulated by DEAF1 were also reduced in GVHD, we used gene set enrichment analysis (GSEA) to determine enrichment or otherwise of 157 DEAF1-dependent genes (defined as genes with ≥ 3-fold reduced expression in LN stromal cells from *Deaf1* knockout versus wild type mice) (18). As shown in Figure 1D, GVHD was associated with down-regulation of this gene set in FRC (normalised enrichment score -2.45 FDR q value=0.0007 for TCDBM+T versus TCDBM comparison). Down-regulation of DEAF1-dependent genes in FRC was specific to GVHD and not generalizable to BMT alone, or to LN FRC responses to other inflammatory stimuli, including to HSV infection (27) or to IL-17 following vaccination (28). Finally, we used RT-PCR to evaluate how GVHD affected the expression of specific PTA genes known to be expressed by FRC (*Mlana*, *Plp* and *Rrad*) (15); as shown in Figure 1E, *Mlana* (encoding melan-A, expressed in skin) was significantly reduced with a similar trend for *Rrad* (encoding ras related glycolysis inhibitor and calcium channel regulator, expressed in muscle and lung) but not for *Plp* (encoding proteolipid 1, expressed in brain). Thus, FRC show a complex acute transcriptional response to GVHD that includes early down-regulation of genes critical to their core functions in supporting survival of naïve T cells as well as their role in the peripheral display of PTA.

Damage to the FRC network following acute GVHD is irreversible

Intra-nodal PTA display in GVHD will be affected not only by expression levels of relevant antigens by individual stromal cells but also on the overall integrity of each of the populations. To address how acute GVHD would impact upon peripheral LN stroma overall, we tracked stromal numbers over time in the F→M BMT model. Using the gating strategy shown in Figure 2A, we found that FRC numbers progressively fell by ~10-fold following the onset of GVHD over several weeks with no evidence of recovery at 18 weeks; in contrast, other major stromal populations, lymphatic endothelial cell (LEC) and blood endothelial cell (BEC) numbers remained intact (Figure 2A-B). Loss of FRC was confirmed by confocal immunofluorescence imaging and associated with marked disruption of LN paracortex structure (Supplementary Figure 2A). The extent of FRC depletion (compared to baseline) was less if MataHari T cells were transferred after a delay of 7 days, a

situation where the severity of GVHD is significantly reduced (32), indicating that the degree of alloreactivity is important in dictating injury to this population (Figure 2C). To test if FRC targeting in this $CD8^+$ T cell-dependent model required cognate interaction with MHC Class I-expressing target cells, we established BM chimeras where radioresistant stromal cells either did or did not express MHC Class I (i.e. [B6 male → B6 male] versus [B6 male → *B2m*$^{-/-}$ male] BM chimeras, respectively) and then, induced GVHD following a 2nd BMT. As shown in Figure 2D, lack of MHC Class I expression by stroma protected the FRC population from GVHD-induced injury. As previously demonstrated following acute LCMV infection (26), $CD8^+$ T cell targeting of FRC in acute GVHD was independent of the perforin pathway (Supplementary Figure 2B). However, MHC Class I-restricted targeting of FRC was not required for their elimination as HY-specific $CD4^+$ T cells could also induce FRC loss following F→M BMT, albeit that the extent of injury was less than observed in the $CD8^+$ T cell-dependent model (Supplementary Figure 2C). The long time frame afforded by the MataHari model (survival is ~50% at 18 weeks in mice with GVHD) allowed us to determine if FRC regeneration could occur if acute GVHD was terminated early during its evolution. In the Ccl19.DTR model, administration of diphtheria toxin (DT) induces complete ablation of the FRC population with partial recovery evident at 2 weeks and almost full recovery at 4 weeks (33). Thus, we sought to measure the long-term integrity of the FRC network under conditions where GVHD had been terminated at an earlier time point using anti-CD8α antibody depletion following BMT and T cell transfer (Supplementary Figure 2D shows the effect of anti-CD8α antibody upon clinical GVHD; median $CD8^+$ T cell numbers at 4 weeks were 4.23% of live gate in control versus 0.007% in antibody-treated mice, $p<0.0001$, Mann-Whitney test, 2-tailed). If anti-CD8α antibody was given from day 5 after BMT (a time point when the majority of the FRC network remains intact; Figure 2B), we found that FRC numbers were preserved to a similar extent as controls without GVHD when evaluated at the 4-week time point (Figure 2E). We next asked whether FRC network could recover if GVHD was terminated at the later time point of day 14 when substantial loss of the FRC population had already occurred (Figure 2B). As shown in Figure 2F, if the start of anti-CD8α antibody treatment was delayed to 14 days after BMT and T cell transfer,

FRC numbers did not recover over the next 5 weeks in the CD8-depleted mice when compared to controls without GVHD. A slight trend for increased in FRC numbers in the CD8-depleted compared with the non-depleted group was observed at the 2 week time point indicative of less exposure to the process causing immune injury and/or an abortive attempt at recovery, but this effect was only transient. Together, these data indicate that the capacity for the FRC network to remain intact is dependent upon the extent and/or duration of injury induced by GVHD; the longer the duration of injury, the lower the capacity for FRC regeneration.

We next addressed how clinical strategies designed to prevent or treat GVHD in human patients would impact upon the integrity of the LN FRC population. In these experiments, we employed a clinically relevant MHC-matched (H-2^b), multiple minor antigen mismatched model of BMT (B6→129) where GVHD is more severe than the F→M model (survival 40-50% at 3 weeks). We found that GVHD induced similar damage to the FRC network as in the F→M model, with a reduction of ~10-fold by day 21 compared to BMT recipients without GVHD. LEC numbers were also reduced at this time point but only by ~2-fold (Figure 3A). Clinical prevention of human GVHD can be achieved by selective removal of naïve T cells from the graft, thus depleting T cells with the greatest potential for alloreactivity (34). Because CD62L expression is required for trafficking of naïve T cells to LN following experimental BMT (35), we reasoned that removal of $CD62L^+$ cells from donor input T cells would also prevent damage to the FRC network. Transfer of $CD62L^-$ T cells was effective at preventing GVHD in the B6→129 BMT model (Supplementary Figure 3A) and also induced significantly less depletion of the FRC population than non-manipulated T cells (Figure 3B); this effect was also observed when the input T cell numbers were adjusted to allow equal representation of $CD4^+$ and $CD8^+$ T cell subsets between the experimental cohorts (data not shown). A second widely adopted strategy for preventing GVHD is the use of post-transplant cyclophosphamide (PTCy) which involves administration of a short pulse of cyclophosphamide, usually on days 3-4 following infusion of an un-manipulated graft (36). In pre-clinical models, PTCy depletes or inactivate rapidly dividing alloreactive T cells, while preserving

non-alloreactive T cells and regulatory T cell (Treg) numbers (37, 38). We found that administration of cyclophosphamide at a dose of 25 mg/kg on days 3 and 4 following B6→129 BMT and T cell transfer, partially reduced clinical GVHD scores and donor T cell expansion (Supplementary Figure 3B); however, the extent of FRC loss on day 18 was similar to GVHD controls (Figure 3C). We next addressed whether treatment of GVHD could allow subsequent recovery of the FRC population by adapting the B6→129 model to incorporate corticosteroids as used routinely in the clinic (1). Thus, we treated BMT recipients with 0.3 mg/kg/day intraperitoneal dexamethasone or PBS starting from day 5 after BMT and co-transfer of donor T cells; FRC numbers were assessed 2 weeks after treatment initiation (day 19 post BMT). Dexamethasone treatment partially reduced the clinical GVHD score and donor T cell expansion, and led to a modest improvement in survival (Supplementary Figure 3C); however, FRC numbers fell to a similar extent as in GVHD control mice (Figure 3D). Of note, corticosteroid treatment alone over an equivalent period in non-BMT mice did not lead to reductions in FRC numbers excluding any direct drug toxicity (Supplementary Figure 3D). Taken together with the results from Figure 2E, where robust CD8-depletion from day 5 offered almost full protection in the F→M BMT model, we reason that the failure of PTCy or corticosteroids to protect against FRC loss relate to their incomplete activity in blocking residual alloreactivity in the B6→129 model.

Acute GVHD blocks stromal re-organisation and repair of the FRC network

Our finding here that FRC population recovery was impaired following initial injury suggested the disruption of critical repair mechanisms required for LN stromal reconstruction. To determine whether FRC loss triggered a re-organisational transcriptional signature as seen in acute viral infection (26), we flow sorted FRC cells derived from mice developing acute GVHD and controls on day 7 in the MataHari F→M model and performed RNAseq. As shown in Figure 4A, the expression of reorganisation genes (e.g. *Vcam1, Icam1, Cxcl13, Ltbr*) was significantly reduced in GVHD mice compared to controls, suggesting that molecular interactions characteristic of cross-talk between LTo and LTi cells had been disrupted. To discern if GVHD-induced FRC injury

provoked a similar influx of LTi as observed in viral infection, we next tracked numbers of LTi cells (defined as lineage$^-$CD117$^+$IL-7Rα^+RORγt$^+$) in both the F→M models and B6→129 models (see Supplementary Figure 4A for gating strategy), using congenic markers to identify their host/donor origin. LTi populations were negative for expression of NKp46 but positive for CCR6, consistent with their lymphoid organ location (Supplementary Figure 4A). As shown in Figure 4B (F→M model) and Supplementary Figure 4B (B6→129 model), the host LTi population was partially replaced over several weeks by donor-derived LTi in the absence of acute GVHD. In contrast, we observed a biphasic pattern in GVHD mice involving an initial trend for host LTi to be present in greater numbers (around day 7) compared with controls, but the almost complete elimination of the population (both host and donor-derived) at later time points. To determine how acute GVHD would affect stromal reorganisation, we evaluated BMT mice for the presence of activated LTo-like cells (defined as CD45$^-$VCAM1^{high}ICAM1^{high}), akin to those required for embryonic LN development (19). As shown in Figures 4C (F→M model) and Supplementary Figure 4C (B6→129 model), acute GVHD led to an early trend (day 2 in the F→M model and day 7 in the B6→129 model) for an increase in the frequency of the CD45$^-$VCAM1^{high}ICAM1^{high} population but, in both models, this early increase was not sustained compared to BMT mice without acute GVHD (Figure 4C). One possible explanation for the failure to invoke a sustained FRC repair program in acute GVHD was the failure to maintain LTi numbers in the peripheral LN, thus impairing crosstalk with FRC or their LTo-like precursors. To determine whether lack of host LTi cells would increase the extent of FRC loss as reported for acute LCMV infection (26), we adapted our F→M model to eliminate host LTi by using recipient mice that lack RORγt (encoded by the gene *Rorc*), a transcription factor which is required for LTi development (39). Thus, we compared FRC numbers following induction of GVHD following secondary BMT in established [male *Rorc wt* →male *Rorc wt*] or [male *Rorc ko* →male *Rorc wt*] BM chimeras, the latter chimeras lacking LTi. As shown in Figure 4D, although host LTi cells were absent in established [*Rorc ko* →*Rorc wt*] chimeras before the second BMT, we observed no difference in the baseline numbers of FRC (Figure 4D). Furthermore and in contrast to acute LCMV infection (26), the absence of host LTi did not increase the extent of FRC injury

following subsequent induction of acute GVHD in a secondary F→M BMT (Figure 4E). Neither MataHari T cell expansion nor acute GVHD severity was affected by the absence of RORγt$^+$ cells (data not shown). Together, these data show that the normal repair mechanism for FRC restoration is profoundly impaired in acute GVHD. However, unlike acute LCMV infection, host LTi are redundant in protecting the FRC network from injury.

Autoreactive T cells fail to be purged from the periphery in acute GVHD

Our findings that GVHD induced early PTA gene down-regulation in FRC (Figure 1D and E) and subsequent elimination of almost the entire FRC population (Figures 2 and 3) suggested that intra-nodal display of PTA would be severely disrupted. We reasoned that defects in peripheral PTA presentation would increase the risk that autoreactive T cells would develop effector functions capable of inducing tissue injury. To test this hypothesis, we used a model antigen system where PTA display by lymph node stromal cells is critical for peripheral tolerance of autoreactive T cells. Thus, we adapted the iFABPtOVA model in which a transgene encodes a truncated cytosolic form of OVA (tOVA) regulated by the promoter for intestinal fatty acid binding protein (iFABP) leading to the expression of the model self-antigen in intestinal epithelial cells (40). In this model, radioresistant LN stromal cells can directly present OVA to induce abortive proliferation and deletion of OVA-specific OT-I CD8$^+$ T cells, thus preventing intestinal inflammation (15, 16). Among the LN stromal cells, expression of OVA is restricted to the FRC population suggesting that this population is critical for tolerance (15). We hypothesized that development of acute GVHD in iFABPtOVA mice would abrogate this putative tolerance mechanism as a result of FRC depletion and loss of LN display of the model PTA. We therefore induced acute GVHD in iFABPtOVA male BMT recipients by co-transfer of female TCDBM and Mh CD8$^+$ T cells (Figure 5A); additional male OVA-negative B6 recipients undergoing F→M BMT with or without acute GVHD served as controls. Similarly to non-transgenic BMT recipients, development of acute GVHD in iFABPtOVA mice reduced total FRC numbers by 14 days post BMT compared with GVHD$^-$ iFABPtOVA controls (Supplementary Figure 5A); intra-nodal expression of the model self-antigen OVA by

residual FRC was also reduced in GVHD mice (Supplementary Figure 5A). At 6 weeks following BMT, when the acute effects of irradiation had resolved, the integrity of the peripheral tolerance mechanism to intestinal OVA was evaluated in each group by transferring 10^6 OT-I T cells, which were then tracked as a surrogate for autoreactive T cells (Figure 5A). By day 16 following OT-I T cell transfer, $GVHD^+$ iFABPtOVA BMT recipients showed significant weight loss compared with $GVHD^-$ iFABPtOVA controls (Figure 5B). OT-I transfer had no effect upon the weight of OVA-negative $GVHD^+$ B6 recipients indicating that the weight loss in $GVHD^+$ iFABPtOVA mice was antigen-specific (Figure 5B). To investigate whether weight loss in $GVHD^+$ iFABPtOVA BMT recipients was due to a failure to purge transferred OT-I effector cells from the periphery, we measured OT-I numbers and functions in LN and small intestine. As shown in Figure 5C, transferred OT-I T cells were detectable at significantly higher frequencies in the peripheral LN (PLN, Supplementary Figure 5B), mesenteric LN (mLN) and the intraepithelial lymphocyte compartment (IEL) of $GVHD^+$ iFABPtOVA mice compared with $GVHD^-$ iFABPtOVA controls (Figure 5C; B6 BMT controls with and without GVHD are shown in Supplementary Figure 5C). Consistent with the disruption of FRC network upon LN integrity and the expected reduction in global LN T cell numbers (24, 25), absolute numbers of OT-I T cells were lower in the mLN $GVHD^+$ iFABPtOVA mice than in $GVHD^-$ controls; however, OT-I absolute numbers were significantly increased in the small intestine IEL (Figure 5D). To determine the functions of the OT-I T cell population, we measured cytokine generation by OT-I T cells in PLN (Supplementary Figure 5B), MLN and IEL from each group following brief *ex vivo* re-stimulation. As shown in Figure 5E and F, MLN and IEL OT-I T cells from $GVHD^+$ iFABPtOVA mice expressed higher quantities of IFNγ compared with controls indicating a failure to block T cell autoreactivity in acute GVHD. OT-I frequency and absolute numbers were not increased in the small intestine IEL of OVA-negative $GVHD^+$ B6 BMT recipients indicating that bystander expansion and trafficking of OT-I cells in the absence of antigen did not occur (Supplementary Figure 5C).

Although tolerance in the iFABP-tOVA model occurs through peripheral deletion, surviving OT-I T cells may still retain the ability to induce intestinal injury if cross-primed by professional antigen-

presenting cells during an unrelated inflammatory process (40, 41). Furthermore, it has recently been shown that donor-derived, migratory $CD103^+$ $CD11b^-$ dendritic cells (DC) can aggravate intestinal inflammation in acute GVHD by cross-presenting host antigens in the early phase (<2 weeks) following allogeneic BMT (42). We therefore sought to determine whether cross-presentation of intestinal OVA antigen by donor DC could also be disrupting loss of peripheral tolerance in $GVHD^+$ iFABPtOVA mice by adapting the experimental model to allow depletion of donor DC. Thus, irradiated iFABPtOVA mice were reconstituted with BM from CD11cDTR mice (43), allowing the specific depletion of $CD11c^+$ DC upon DT administration at the point of transfer of OT-I T cells 6 weeks following BMT. As shown in Figure 5G and H, depletion of DC by intra-peritoneal injection of DT every third day starting on day 41 following BMT (Supplementary Figure 5D) and transfer of OT-I T cells on day 42 had no effect upon the subsequent effector function of OT-I measured by secretion of IFNγ in MLN and IEL 16 days later. Thus, both in the absence and presence of donor DC, OT-I T cells isolated from $GVHD^+$ iFABPtOVA recipients showed equivalent elevation in IFNγ expression compared with $GVHD^-$ iFABPtOVA mice. Taken together, these data demonstrate a failure to purge autoaggressive T cells in the periphery following the development of acute GVHD through mechanisms that are independent of enhanced cross-presentation of self-antigens by donor DC.

Loss of FRC is sufficient to break peripheral tolerance of autoreactive T cells

Because multiple mechanisms could potentially explain loss of peripheral tolerance in the context of inflammation, it was possible that FRC network injury was unrelated to the auto-aggressive behaviour of OT-I T cells in $GVHD^+$ iFABPtOVA mice. We therefore asked whether the loss of FRC in a non-inflammatory environment in mice without GVHD would be sufficient to disrupt peripheral tolerance induction in LN. We therefore crossed iFABPtOVA and Ccl19cre.DTR (24) (OVA.Ccl19.DTR) mice to allow for DT-mediated depletion of $Ccl19^+$ FRC in the absence of GVHD. During the 3-week course of the experiment, DT treatment of OVA.Ccl19.DTR mice on days -8, -6, -4, +2, +6, +9 and +13 led to long-lasting (>95%) depletion of FRC (Figure 6A, B). As

shown in Figure 6C, transfer of OT-I cells to recipient mice led to transient weight loss in the FRC-depleted cohort peaking at day 7. As we observed in GVHD$^+$ iFABPtOVA recipients, transferred OT-I T cells were detectable at significantly higher frequencies in both mLN and IEL of FRC-depleted host compared with FRC-replete controls (Figure 6D). Similar to the GVHD model, absolute numbers of OT-I T cells were also increased in the IEL when FRC were depleted (Figure 6E) and this was associated with increased numbers of IFNγ-secreting cells in both the mLN and IEL (Figure 6F and G). Thus, these experiments identify the FRC population as being specifically required for peripheral tolerance of autoreactive CD8$^+$ T cells in the iFABPtOVA model. Furthermore, these data show that FRC elimination is sufficient to trigger auto-aggressive T cell behaviour even in the absence of inflammation, a scenario where other peripheral tolerance mechanisms are anticipated to remain intact. Thus, although GVHD may disrupt multiple regulatory mechanisms in the periphery, these data indicate that FRC network damage contributes to the loss of tolerance to PTA.

FRC express a distinct PTA gene signature enriched for genes normally expressed in target organs of chronic GVHD.

Because it has been shown that individual LN stromal cell subsets each express a distinct repertoire of PTA (14, 15), we next sought to characterize the nature of an FRC-specific PTA signature in non-transgenic mice by analysing transcriptional profiles for individual, steady state LN stromal cell subsets using published data from the Immgen consortium (29) (a summary of the analytical pipeline is shown in Figure 7A). Putative PTA were identified on the basis of their transcription in <5 different tissues (9, 12, 44) and gene expression within the top quartile for pooled LN stromal cell data (n=1494 genes). PTA gene expression in FRC was distinct from LEC and BEC, whereas LEC and BEC PTA gene expression was very similar (Figure 7B). Based upon a comparison of PTA gene expression between the different LN stromal cell subsets (Figure 7B), we identified a list of 356 putative FRC-specific PTA genes based upon ≥3-fold greater expression and an adjusted p-value ≤ 0.05 compared with the other LN stromal subsets (listed in

Supplementary Table S1). Of note, when we evaluated in which tissues each of these genes was expressed, we found that 246/356 genes (69.1%) of the PTA genes were also expressed in known target tissues affected by chronic GVHD (skin epidermis, cornea, lacrimal gland, gut, liver, salivary gland, tongue epidermis, skin epidermis, lung, skeletal muscle); this same level of enrichment was not observed in a randomly selected set of 356 non-FRC specific PTA genes expressed in LN stromal cells where 187/356 (52.2%) of genes were expressed in chronic GVHD target tissues ($p<0.0001$, Fisher's exact test; Figure 7C). We also compared the FRC PTA gene set with 283 PTA genes that are normally expressed by thymic mTEC but whose expression is reduced (>3-fold) following the onset of acute GVHD (9). Although the overlap in gene sets was slightly greater than expected (8 overlapping genes from a total of 6611 PTA genes (44), a 2.1-fold increase over expected, $p=0.012$ by hypergeometric testing), the vast majority of genes (>97%) were specific to either the mTEC or FRC compartment (Figure 7D). Akin to the acute down-regulation of known PTA genes shown in Figure 1E, GSEA showed acute down-regulation of the FRC-specific PTA gene set in FRC cells sorted on day 7 following the onset of acute GVHD in the F→M BMT model (NES -14.4, FDR q value= 0; Figure 7E). On day 7, the majority of the FRC population remained intact (Figure 2B) and these early reductions in gene expression were not indicative of a global depression in gene transcription because expression of a random list of non-PTA genes in FRC showed heterogeneous changes in gene expression compared with controls (Supplementary Figure 6). Furthermore, PTA gene expression was also specific to acute GVHD and did not occur when FRC were exposed to other inflammatory stimuli (Figure 7E). Taken together, these data indicate that acute GVHD rapidly disrupts intra-nodal display of a unique PTA gene set that mirrors the repertoire of genes expressed in the target organs of chronic GVHD.

Discussion

We have shown that acute GVHD damages the FRC network in LN, as well as its capacity for regeneration. Unlike FRC loss accompanying acute LCMV infection, which is associated with a rapid influx of LTi and induction of LN re-organisation (26), no similar process is evident in GVHD and LTi provide no protection. While FRC loss is known to be associated with immune deficiency (24, 25), we find here that the same process can also lead to simultaneous autoimmunity. Thus, early down-regulation of putative PTA gene expression in FRC, followed later by physical loss of the FRC network, impedes peripheral education of autoreactive T cells and allows tissue injury to occur. Together with the known impact of acute GVHD upon thymic education, our data provide support for a 'two hit' model in which defects in both central and peripheral PTA display allow autoimmunity to break through and perpetuate chronic inflammation.

FRC network injury was consistently observed in several models of acute GVHD although, in contrast to a previous report (21), we also observed FRC damage in a purely $CD4^+$ T cell-dependent model, consistent with the up-regulated expression of MHC class II upon FRC in the context of an inflammatory stimulus (29). These data indicate an inherent FRC sensitivity to immune injury compared with other LN stromal cell populations. Although we observed some differences, we observed very similar changes in gene expression in FRC early following acute HSV infection (27), including increased representation of pathways related to apoptosis. In contrast to GVHD, HSV infection is not ultimately associated with net loss of the FRC network. Thus, our findings suggest default components of the transcriptional response of FRC to diverse inflammatory stimuli; these changes are consistent with a requirement for FRC population expansion to accommodate a rapidly developing immune response and a counter-regulatory increase in susceptibility to apoptosis allowing a subsequent return to homeostasis. However, in the context of acute GVHD, homeostasis cannot be restored because of ongoing immune injury and/or the failure of physiological FRC network repair mechanisms.

It has been proposed that FRC network repair following acute LCMV infection triggers a re-organisational program that recapitulates the LTi-LTo interaction required for LN organogenesis in the embryo (26). We explored whether a similar process occurs following injury imposed by acute GVHD. Although host LTi were radio-sensitive, we observed an initial trend for greater LTi persistence compared to controls as well as a transient increase in the frequency of a $CD45^{-}VCAM^{hi}ICAM^{hi}$ population akin to the phenotype of activated LTo-like cells; however, neither population was sustained and both cell types were severely depleted compared with non-GVHD controls at later time points. Our data therefore indicate that FRC injury in acute GVHD leads to an abortive reorganizational program distinct from the process occurring following acute LCMV infection. Indeed, we found that host-derived LTi were redundant in protecting the FRC population unlike the situation reported for acute LCMV (26). Similarly, we observed no increase in the frequency of LTi or $VCAM1^{hi}ICAM1^{hi}$ cells following transient depletion of FRC in Ccl19.DTR mice where network destruction occurs in the absence of inflammation (data not shown). There is therefore a need to better define the constituent elements that normally permit stromal regeneration in adults according to the precise context in which FRC network degeneration occurs.

Although the global transcriptional response of FRC in acute GVHD and other inflammatory stimuli was similar overall, acute down-regulation of a putative FRC-specific PTA gene set occurred only following the onset of acute GVHD. Protein expression of PTA in LN stromal populations is usually below the limits of detection so that the peripheral display of PTA antigens other than the model antigen we used has to be inferred. The ectopic expression of genes encoding PTAs in pancreatic LN stromal cells is regulated in part by DEAF1 (18); this transcriptional regulator has structural homology to AIRE, containing a DNA-binding SAND (Sp100, AIRE-1, NucP41/75, and DEAF1) domain, which mediates chromatin-dependent transcription and protein–protein interactions and a ZF-MYND (zinc finger, myeloid, Nervy, and DEAF1) domain that is similar to the plant homeodomain 1 of AIRE. DEAF1 controls the transcription of PTA but also regulates their processing and presentation by controlling expression of eukaryotic translation initiation factor 4 gamma 2 (45). *Deaf1* gene expression was reduced early in FRC following acute GVHD onset

and this change was coincidental with reduced PTA gene expression. Indeed, we found a significant overlap between genes down-regulated in LN stroma of *Deaf1* knock out mice and FRC in acute GVHD although this comparison is limited by differences in mouse strains used to identify regulated genes (Balb/c for *Deaf1* knock out because B6 strain are not viable after birth) and the relative lack of purity of the stroma analysed (18). The lack of overlap between the FRC-specific set of 356 PTA genes we defined here and the gene set previously identified as being regulated by DEAF1 (data not shown) may also relate to these same issues, although other mechanisms may exist for PTA gene regulation in the LN. Future studies involving FRC-specific deletion of *Deaf1* will provide further insight as to whether its down-regulation in acute GVHD is solely responsible for reduced PTA expression. Furthermore, the recent finding that lymph node innate lymphoid cells type 3 (ILC3) express AIRE (46) and the permanent depletion of ILC3-related LTi population in GVHD shown here could suggest a more general deficit in peripheral antigen display than accountable by injury to the FRC network alone.

The FRC PTA gene set we defined from steady state FRC was distinct from that expressed by other LN stromal populations and enriched for genes expressed in the classical target organs of chronic GVHD. Because there are no available GVHD models that fully recapitulate the transition from acute to chronic GVHD, we employed the more tractable iFABPtOVA system to test the hypothesis that loss of FRC antigen display would increase the frequency and functions of autoreactive T cells (40). This model system was chosen because radioresistant LN stromal cells have been shown to directly present OVA to induce tolerance through abortive proliferation and deletion of OVA-specific OT-I $CD8^+$ T cells (15, 16). We showed that purging of autoreactive $CD8^+$ T cells from the peripheral repertoire in iFABPtOVA mice was abrogated several weeks following the onset of acute GVHD through a mechanism that was independent of increased cross-presentation of OVA by dendritic cells in gut-draining LNs. Although it is likely that the inflammatory environment of GVHD impairs other peripheral regulatory mechanisms (e.g. Treg), depletion of FRC in the absence of inflammation was able to reproduce the same degree of autoreactivity as observed in GVHD indicating that this mechanism alone is sufficient to break

tolerance. It is important to note that we evaluated this loss of peripheral tolerance in only one model system where alloreactive T cells (HY-specific MataHari), autoreactive T cells (OT-I) and recipient mice expressing a model TRA in FRC (iFABPtOVA) were all on a B6 background. It will be important therefore to validate our findings in independent model involving other PTAs or other strain backgrounds; in turn, this will depend upon the development of tractable systems where autoreactive T cells with reactivity to FRC-expressed PTA can be tracked. How GVHD-induced disruption to the LN architecture impacts upon other regulatory mechanisms will also be important to explore, particularly in relation to stromal MHC Class II-restricted expression of PTA or the survival of other regulatory populations. For example, it has recently been reported that FRC can suppress intestinal injury by regulating the functions of ILC1 in gut-associated lymphoid tissue when triggered by inflammation (47). While this mechanism could conceivably contribute to evolution of intestinal GVHD, ILC1 also require steady state trans-presentation of IL-15 by FRC for their survival (47); thus, the loss of tolerance in iFABPtOVA mice we observed following inducible FRC depletion in the absence of an inflammatory stimulus (Figure 6) is unlikely to be dependent upon ILC1 activation.

A key question is how current or emerging clinical strategies to prevent or treat GVHD will impact upon the FRC population and peripheral tolerance. Individual strategies will differ in the extent to which they prevent initial damage to the FRC network, block ongoing immune injury or preserve repair/regeneration pathways. It is unlikely therefore that this process is 'all-or-none' and we reason that the level of injury caused by GVHD will vary in human patients according to multiple factors. In addition, the animal models presented here do not fully re-capitulate the clinical setting (e.g. the use of calcineurin inhibitor drugs) or were found to be associated with incomplete inhibition of the alloreactive response (e.g. as shown for PTCy and corticosteroid treatment). Furthermore, some approaches may be better at promoting other peripheral tolerance mechanisms (e.g. expansion of Treg with PTCy (37, 38)) that could compensate for loss of peripheral education of autoreactive T cells by FRC. Indeed, it is also possible that such tolerance

mechanisms will ultimately enable regenerative/repair pathways to re-emerge and restore FRC integrity even if initial injury has occurred.

In conclusion, our data highlight the importance of loss of regeneration/repair mechanisms as being an important driver of GVHD. While injury to epithelial stem cells in acute GVHD is the most overt example of this phenomenon (48, 49), lack of stromal repair within lymphoid organs (both thymus and LN) disrupts the normal mechanisms of T cell development and education leading to the paradoxical co-existence of immunodeficiency and autoimmunity. Future strategies designed to ensure continuous PTA display in the periphery by protection or regeneration of LN stroma may be essential to breaking the transition from acute to chronic GVHD.

Materials and methods

Mice

C57BL/6 (B6), 129/Sv and *Pfp*$^{-/-}$ mice were purchased from Charles River Laboratories and bred in house by UCL Biological Services. *B6 CD45.1 mice,* OT-I *Rag1*$^{-/-}$ mice, *CD11c.DTR mice, B2m*$^{-/-}$ *mice and* ROSA26.iDTR mice were purchased from the Jackson Laboratory. Marilyn (50) and MataHari mice (51) were provided by Jian Chai (Imperial College London, London, UK) and bred in house. iFABPtOVA mice were originally generated by Leo Lefrançois at University of Connecticut (40) and provided by Simon Milling (University of Glasgow, UK). *Ccl19.cre* mice were provided by Burkhard Ludewig (Kantonal Hospital St. Gallen, Switzerland) (24) and bred in house by crossing with iFABPtOVA and/or ROSA26iDTR mice. All procedures were conducted in accordance with the United Kingdom Home Office Animals (Scientific Procedure) Act of 1986 and were approved and performed according to the Animal Welfare and Ethical Review Body of the Comparative Biology Unit Royal Free Hospital and University College London Medical School.

Flow cytometry

The following anti-mouse surface antibodies were used: CD45 (clone 30-F11, BioLegend, USA), gp38 (8.1.1, BioLegend), CD31 (MEC13.3, BioLegend), ICAM1 (clone YN1/1.7.4, BioLegend), VCAM1, (clone 429 (MVCAM.A), BioLegend), CD8 (53-6.7, BD Biosciences, Germany), CD4 (RM4-4, eBioscience, USA), Vα2 (B20.1, eBioscience), Vβ5 (MR9-4, eBioscience), CD45.1 (A20, BD Biosciences), CD90.1 (Thy1.1, clone HIS51, eBioscience, USA), CD62L (MEL-14, BD Biosciences), CD44 (IM7, BioLegend), CD69 (H1.2F3, BD Biosciences), Vβ8.3 (1B3.3, BD Biosciences), CD11c (HL3, BD Biosciences), CD11b (M1/70, BioLegend), IA-IE (MHCII, clone M5/114.15.2, eBioscience), CD24 (M1/69, BD Biosciences), CD127 (A7R34, eBioscience), CD117 (2B8MH, BD Biosciences), CD3 (145-2C11, BD Biosciences), CD19 (1D3, BD Biosciences), NK1.1 (PK136, eBioscience), LY6G (1A8, BD Biosciences) CD196 (CCR6; 29-2L17, BioLegend), NKp46 (29A1.4, eBioscience) and F4/80 (BM8, eBioscience). For intracellular cytokine staining, cells were incubated with 10ng/ml phorbol 12-myristate 13-acetate (PMA; Sigma, UK) and 1µg/ml

ionomycin (Sigma, UK) in the presence of 1µg/ml brefeldin A (Sigma, UK) for 4h at 37°C before fixation and permeablization (BD Cytofix/Cytoperm, BD Biosciences, UK), followed by incubation with antibody against IFNγ (XMG1.2, BD Biosciences). Intracellular RORγt (Q31-378, BD Biosciences) staining was carried out in non-stimulated cells using the Foxp3/Transcription Factor Staining Buffer Set (eBiosience). Cells were acquired on a BD LSRFortessa Cell Analyzer (BD Biosciences, UK) and analysed using FlowJo v10 (TreeStar, Ashland, OR, USA). Cells were sorted on a BD FACS Aria IIu cell sorter (BD Biosciences, UK).

Bone marrow transplantation

Single miHA mismatch HY-specific model: BMT was performed as described previously (30, 32). Briefly, to induce acute GVHD,, male C57BL/6 (B6; H-2^b) or iFABPtOVA (H-2^b) recipient mice were lethally irradiated (11Gy total body irradiation) and reconstituted with $5x10^6$ TCDBM, $2x10^6$ polyclonal female B6 $CD4^+$ T cells and $1x10^6$ female MataHari $CD8^+$ T cells. No GVHD control recipients received TCDBM alone. Multiple miHA mismatch model: 129/Sv (129; H-2^b) were used as recipients. Acute GVHD was induced by transferring $5x10^6$ TCDBM, $2x10^6$ $CD4^+$ and $1x10^6$ $CD8^+$ T cells (all from B6 donors). No acute GVHD controls received TCDBM alone. T-cell depletion of BM through negative selection and isolation of $CD4^+$ and $CD8^+$ T cells (including OT-I cells) by positive selection was performed using manual MACS Cell Separation (CD4 (L3T4) MicroBeads and CD8α (Ly-2) MicroBeads; Miltenyi Biotec, Germany) according to the manufacturer's instructions. Negative selection of $CD62L^+$ cells was performed using CD62L microbeads (Miltenyi Biotec, Germany). For in vivo CD8 depletion, 1.44 mg of anti-CD8α depleting antibody (Bio X Cell, West Lebanon, NH, USA) was given by i.p. injection and repeated after 2 weeks. Dexamethasone (Wockhardt, UK) treatment started on day 5 post transplant and was given daily by i.p. injections (0.3 mg/kg/day) until take down. Post-transplant cyclophosphamide (PTCy; Sigma, UK) was given by i.p. injection on days 3 and 4 at 25 mg/kg/day.

Cell isolation

LN stromal cells were isolated from peripheral and mesenteric LN at indicated time points after transplantation or diphtheria toxin (DT) treatment and enzymatically digested with 0.2mg/ml Liberase TM (Roche Diagnostics, Switzerland) and 20µg/ml Dnase (Sigma, UK) in PBS at 37°C for 30min with mechanical disruption every 5min. Supernatants containing stroma cells were collected and enzyme mix was replaced. LN, spleen and small intestine cells were isolated at indicated time points using methods described previously (30, 32). Cells were counted using a CASY Model TT – Cell Counter and Analyzer (Roche, Penzberg, Germany).

RNA sequencing and analysis

RNA was amplified using the SMART Seq v4 Ultra Low Input RNA kit (Takara Bio, Mountain View CA, USA) and cDNA libraries were prepared according to the Nextera XT DNA Library Preparation kit protocol (Illumina, USA). Sequencing was performed on a Illumina NextSeq 500 (Illumina), generating >15million 38bp paired end reads per sample. Adapter trimming of the reads was performed by FASTQ Toolkit. Alignment and library mapping were performed using TopHat Alignment and Cufflinks Assembly & DE. Gene expression levels and differentially expressed genes were calculated using Cufflinks/Cuffdiff. Data is available on www.ebi.ac.uk/arrayexpress, accession number E-MTAB-8255.

Identification of peripheral tissue-restricted antigens (PTA)

PTA genes were defined as genes being expressed in <5 tissues as previously described (9, 44). Briefly, gene expression data from public databases Mouse GNF Mouse GeneAtlas V3 (http://biogps.org) was used to define PTA. The published list of PTA with tissue-restricted expression by Sansom et al. 2014 was used for downstream analysis (44). To analyse PTA expression in LN stromal cells, published microarray data was used (29). PTA with high expression in FRC (top quartile) and >3-fold higher expression compared to other LN stromal cell subsets were defined as “FRC-enriched”.

Gene set enrichment analysis (GSEA)

157 genes were identified as DEAF1-dependent based on >3-fold higher expression in wildtype animals compared to *Deaf1-ko* animals and defined as "DEAF1 gene set" (18). 84/157 genes were present in RNAseq data from FRC isolated from mice with or without acute GVHD. Enrichment of the "DEAF1 gene set" in TCDBM vs. TCDBM+T FRC was performed using GSEA software (52). GSEA in naïve FRC, FRC post HSV-1 infection or IL-17 exposure, and FRC isolated from $GVHD^+$ or $GVHD^-$ recipients was performed with the gene sets derived from the REACTOME database collected in the Molecular Signatures Database (MSigDB v5.1). Network visualisation was performed using Cytoscape (53).

FRC and DC ablation in vivo

iFABPtOVA, ROSA26iDTR and Ccl19.cre mice were crossed to generate OVA.Ccl19.DTR mice. Cre^+ and Cre^- control mice were injected intraperitoneally (i.p.) with 500 ng of diphtheria toxin (DT; Sigma, UK) on day -8, -6 and -4 prior to OT-I T cell transfer. To maintain FRC ablation, recipients received 500 ng DT i.p. on day 2, 6, 9 and 13. Mice were analysed on day 16. For depletion of donor CD11c, BMT recipient mice received $5x10^6$ BM from CD11cDTR donor mice together with with polyclonal $CD4^+$ and MataHari $CD8^+$ T cells. Six weeks after BMT and day -1 before OT-I T cell transfer, donor DC were depleted upon i.p. injection of 100 ng DT (54). To maintain DC ablation, recipients received 100 ng DT i.p. every 72 hrs.

Immunofluorescence and confocal imaging

For analysis of LN stromal cells by confocal microscopy, LN were isolated at day 7 after transplantation and frozen in OCT (Cellpath). 8 µm sections were cut on a cryostat, dried and fixed with acetone (-20°C). Primary antibodies were CD31 FITC (clone MEC13.3, BD Biosciences) and gp38 biotin (eBio8.1.1, eBioscience). Secondary antibodies were anti-FITC Alexa 488 (Life Technologies, Oregon, USA) and Streptavidin eFluor570 (eBioscience). Sections were stained with DAPI and mounted with ProLong Diamond Antifade Mountant (Life Technologies). All images were captured on a Nikon Ti inverted microscope using a C2 confocal scan head (Nikon

Instruments, Tokyo, Japan). Images were acquired with a 40x (Plan Apochromat N.A. 0.095 W.D. 0.21 mm) objective. Image analysis was done using the software ImageJ.

Study approvals

All procedures were conducted in accordance with the UK Home Office Animals (Scientific Procedure) Act of 1986, and were approved by the Ethics and Welfare Committee of the Comparative Biology Unit, Hampstead Campus, UCL, London, UK.

Statistics

The nonparametric unpaired Mann-Whitney U test was used for two-group comparisons, whereas for multiple group comparisons Kruskal-Wallis one-way ANOVA with Dunn's post-test was performed using GraphPad Prism (GraphPad Software, La Jolla California USA). A two-tailed p value <0.05 was considered significant.

References

1. Zeiser R, and Blazar BR. Acute Graft-versus-Host Disease - Biologic Process, Prevention, and Therapy. *N Engl J Med.* 2017;377(22):2167-79.
2. Zeiser R, and Blazar BR. Pathophysiology of Chronic Graft-versus-Host Disease and Therapeutic Targets. *N Engl J Med.* 2017;377(26):2565-79.
3. Hollander GA, Widmer B, and Burakoff SJ. Loss of normal thymic repertoire selection and persistence of autoreactive T cells in graft vs host disease. *J Immunol.* 1994;152(4):1609-17.
4. Tivol E, Komorowski R, and Drobyski WR. Emergent autoimmunity in graft-versus-host disease. *Blood.* 2005;105(12):4885-91.
5. Wu T, Young JS, Johnston H, Ni X, Deng R, Racine J, Wang M, Wang A, Todorov I, Wang J, et al. Thymic damage, impaired negative selection, and development of chronic graft-versus-host disease caused by donor CD4+ and CD8+ T cells. *J Immunol.* 2013;191(1):488-99.
6. Zhang Y, Hexner E, Frank D, and Emerson SG. CD4+ T cells generated de novo from donor hemopoietic stem cells mediate the evolution from acute to chronic graft-versus-host disease. *J Immunol.* 2007;179(5):3305-14.
7. Zhao D, Young JS, Chen YH, Shen E, Yi T, Todorov I, Chu PG, Forman SJ, and Zeng D. Alloimmune response results in expansion of autoreactive donor CD4+ T cells in transplants that can mediate chronic graft-versus-host disease. *J Immunol.* 2011;186(2):856-68.
8. Dertschnig S, Hauri-Hohl MM, Vollmer M, Hollander GA, and Krenger W. Impaired thymic expression of tissue-restricted antigens licenses the de novo generation of autoreactive CD4+ T cells in acute GVHD. *Blood.* 2015;125(17):2720-3.
9. Dertschnig S, Nusspaumer G, Ivanek R, Hauri-Hohl MM, Hollander GA, and Krenger W. Epithelial cytoprotection sustains ectopic expression of tissue-restricted antigens in the thymus during murine acute GVHD. *Blood.* 2013;122(5):837-41.

10. Na IK, Lu SX, Yim NL, Goldberg GL, Tsai J, Rao U, Smith OM, King CG, Suh D, Hirschhorn-Cymerman D, et al. The cytolytic molecules Fas ligand and TRAIL are required for murine thymic graft-versus-host disease. *The Journal of clinical investigation.* 2010;120(1):343-56.

11. van den Brink MR, Moore E, Ferrara JL, and Burakoff SJ. Graft-versus-host-disease-associated thymic damage results in the appearance of T cell clones with anti-host reactivity. *Transplantation.* 2000;69(3):446-9.

12. Derbinski J, Gabler J, Brors B, Tierling S, Jonnakuty S, Hergenhahn M, Peltonen L, Walter J, and Kyewski B. Promiscuous gene expression in thymic epithelial cells is regulated at multiple levels. *J Exp Med.* 2005;202(1):33-45.

13. Parkman R. A 2-hit model for chronic GVHD. *Blood.* 2013;122(5):623-4.

14. Cohen JN, Guidi CJ, Tewalt EF, Qiao H, Rouhani SJ, Ruddell A, Farr AG, Tung KS, and Engelhard VH. Lymph node-resident lymphatic endothelial cells mediate peripheral tolerance via Aire-independent direct antigen presentation. *J Exp Med.* 2010;207(4):681-8.

15. Fletcher AL, Lukacs-Kornek V, Reynoso ED, Pinner SE, Bellemare-Pelletier A, Curry MS, Collier AR, Boyd RL, and Turley SJ. Lymph node fibroblastic reticular cells directly present peripheral tissue antigen under steady-state and inflammatory conditions. *J Exp Med.* 2010;207(4):689-97.

16. Lee JW, Epardaud M, Sun J, Becker JE, Cheng AC, Yonekura AR, Heath JK, and Turley SJ. Peripheral antigen display by lymph node stroma promotes T cell tolerance to intestinal self. *Nat Immunol.* 2007;8(2):181-90.

17. Magnusson FC, Liblau RS, von Boehmer H, Pittet MJ, Lee JW, Turley SJ, and Khazaie K. Direct presentation of antigen by lymph node stromal cells protects against CD8 T-cell-mediated intestinal autoimmunity. *Gastroenterology.* 2008;134(4):1028-37.

18. Yip L, Su L, Sheng D, Chang P, Atkinson M, Czesak M, Albert PR, Collier AR, Turley SJ, Fathman CG, et al. Deaf1 isoforms control the expression of genes encoding peripheral tissue antigens in the pancreatic lymph nodes during type 1 diabetes. *Nat Immunol.* 2009;10(9):1026-33.

19. Fletcher AL, Acton SE, and Knoblich K. Lymph node fibroblastic reticular cells in health and disease. *Nat Rev Immunol.* 2015;15(6):350-61.

20. Chung J, Ebens CL, Perkey E, Radojcic V, Koch U, Scarpellino L, Tong A, Allen F, Wood S, Feng J, et al. Fibroblastic niches prime T cell alloimmunity through Delta-like Notch ligands. *J Clin Invest.* 2017;127(4):1574-88.

21. Suenaga F, Ueha S, Abe J, Kosugi-Kanaya M, Wang Y, Yokoyama A, Shono Y, Shand FH, Morishita Y, Kunisawa J, et al. Loss of lymph node fibroblastic reticular cells and high endothelial cells is associated with humoral immunodeficiency in mouse graft-versus-host disease. *J Immunol.* 2015;194(1):398-406.

22. Dilly SA, Sloane JP, and Psalti IS. The cellular composition of human lymph nodes after allogenic bone marrow transplantation: an immunohistological study. *J Pathol.* 1986;150(3):213-21.

23. Nakayama A, Hirabayashi N, Ito M, Kasai K, Fujino M, Ohbayashi M, and Asai J. White pulp reconstitution after human bone marrow transplantation. *Am J Pathol.* 1993;143(4):1111-20.

24. Cremasco V, Woodruff MC, Onder L, Cupovic J, Nieves-Bonilla JM, Schildberg FA, Chang J, Cremasco F, Harvey CJ, Wucherpfennig K, et al. B cell homeostasis and follicle confines are governed by fibroblastic reticular cells. *Nat Immunol.* 2014;15(10):973-81.

25. Denton AE, Roberts EW, Linterman MA, and Fearon DT. Fibroblastic reticular cells of the lymph node are required for retention of resting but not activated CD8+ T cells. *Proc Natl Acad Sci U S A.* 2014;111(33):12139-44.

26. Scandella E, Bolinger B, Lattmann E, Miller S, Favre S, Littman DR, Finke D, Luther SA, Junt T, and Ludewig B. Restoration of lymphoid organ integrity through the interaction of lymphoid tissue-inducer cells with stroma of the T cell zone. *Nat Immunol.* 2008;9(6):667-75.

27. Gregory JL, Walter A, Alexandre YO, Hor JL, Liu R, Ma JZ, Devi S, Tokuda N, Owada Y, Mackay LK, et al. Infection Programs Sustained Lymphoid Stromal Cell Responses and

Shapes Lymph Node Remodeling upon Secondary Challenge. *Cell Rep.* 2017;18(2):406-18.

28. Majumder S, Amatya N, Revu S, Jawale CV, Wu D, Rittenhouse N, Menk A, Kupul S, Du F, Raphael I, et al. IL-17 metabolically reprograms activated fibroblastic reticular cells for proliferation and survival. *Nat Immunol.* 2019;20(5):534-45.

29. Malhotra D, Fletcher AL, Astarita J, Lukacs-Kornek V, Tayalia P, Gonzalez SF, Elpek KG, Chang SK, Knoblich K, Hemler ME, et al. Transcriptional profiling of stroma from inflamed and resting lymph nodes defines immunological hallmarks. *Nat Immunol.* 2012;13(5):499-510.

30. Santos ESP, Cire S, Conlan T, Jardine L, Tkacz C, Ferrer IR, Lomas C, Ward S, West H, Dertschnig S, et al. Peripheral tissues reprogram CD8+ T cells for pathogenicity during graft-versus-host disease. *JCI Insight.* 2018;3(5).

31. Abramson J, and Husebye ES. Autoimmune regulator and self-tolerance - molecular and clinical aspects. *Immunol Rev.* 2016;271(1):127-40.

32. Flutter B, Edwards N, Fallah-Arani F, Henderson S, Chai JG, Sivakumaran S, Ghorashian S, Bennett CL, Freeman GJ, Sykes M, et al. Nonhematopoietic antigen blocks memory programming of alloreactive CD8+ T cells and drives their eventual exhaustion in mouse models of bone marrow transplantation. *The Journal of clinical investigation.* 2010;120(11):3855-68.

33. Novkovic M, Onder L, Cupovic J, Abe J, Bomze D, Cremasco V, Scandella E, Stein JV, Bocharov G, Turley SJ, et al. Topological Small-World Organization of the Fibroblastic Reticular Cell Network Determines Lymph Node Functionality. *PLoS Biol.* 2016;14(7):e1002515.

34. Bleakley M, Heimfeld S, Loeb KR, Jones LA, Chaney C, Seropian S, Gooley TA, Sommermeyer F, Riddell SR, and Shlomchik WD. Outcomes of acute leukemia patients transplanted with naive T cell-depleted stem cell grafts. *J Clin Invest.* 2015;125(7):2677-89.

35. Beilhack A, Schulz S, Baker J, Beilhack GF, Wieland CB, Herman EI, Baker EM, Cao YA, Contag CH, and Negrin RS. In vivo analyses of early events in acute graft-versus-host disease reveal sequential infiltration of T cell subsets. *Blood.* 2005.

36. Kanakry CG, Fuchs EJ, and Luznik L. Modern approaches to HLA-haploidentical blood or marrow transplantation. *Nat Rev Clin Oncol.* 2016;13(1):10-24.

37. Ganguly S, Ross DB, Panoskaltsis-Mortari A, Kanakry CG, Blazar BR, Levy RB, and Luznik L. Donor CD4+ Foxp3+ regulatory T cells are necessary for posttransplantation cyclophosphamide-mediated protection against GVHD in mice. *Blood.* 2014;124(13):2131-41.

38. Wachsmuth LP, Patterson MT, Eckhaus MA, Venzon DJ, Gress RE, and Kanakry CG. Post-transplantation cyclophosphamide prevents graft-versus-host disease by inducing alloreactive T cell dysfunction and suppression. *J Clin Invest.* 2019;129(6):2357-73.

39. Eberl G, Marmon S, Sunshine MJ, Rennert PD, Choi Y, and Littman DR. An essential function for the nuclear receptor RORgamma(t) in the generation of fetal lymphoid tissue inducer cells. *Nat Immunol.* 2004;5(1):64-73.

40. Vezys V, Olson S, and Lefrancois L. Expression of intestine-specific antigen reveals novel pathways of CD8 T cell tolerance induction. *Immunity.* 2000;12(5):505-14.

41. Vezys V, and Lefrancois L. Cutting edge: inflammatory signals drive organ-specific autoimmunity to normally cross-tolerizing endogenous antigen. *J Immunol.* 2002;169(12):6677-80.

42. Koyama M, Cheong M, Markey KA, Gartlan KH, Kuns RD, Locke KR, Lineburg KE, Teal BE, Leveque-El Mouttie L, Bunting MD, et al. Donor colonic CD103+ dendritic cells determine the severity of acute graft-versus-host disease. *J Exp Med.* 2015;212(8):1303-21.

43. Jung S, Unutmaz D, Wong P, Sano G, De los Santos K, Sparwasser T, Wu S, Vuthoori S, Ko K, Zavala F, et al. In vivo depletion of CD11c(+) dendritic cells abrogates priming of CD8(+) T cells by exogenous cell-associated antigens. *Immunity.* 2002;17(2):211-20.

44. Sansom SN, Shikama-Dorn N, Zhanybekova S, Nusspaumer G, Macaulay IC, Deadman ME, Heger A, Ponting CP, and Hollander GA. Population and single-cell genomics reveal the Aire dependency, relief from Polycomb silencing, and distribution of self-antigen expression in thymic epithelia. *Genome Res.* 2014;24(12):1918-31.

45. Yip L, Creusot RJ, Pager CT, Sarnow P, and Fathman CG. Reduced DEAF1 function during type 1 diabetes inhibits translation in lymph node stromal cells by suppressing Eif4g3. *J Mol Cell Biol.* 2013;5(2):99-110.

46. Yamano T, Dobes J, Voboril M, Steinert M, Brabec T, Zietara N, Dobesova M, Ohnmacht C, Laan M, Peterson P, et al. Aire-expressing ILC3-like cells in the lymph node display potent APC features. *J Exp Med.* 2019;216(5):1027-37.

47. Gil-Cruz C, Perez-Shibayama C, Onder L, Chai Q, Cupovic J, Cheng HW, Novkovic M, Lang PA, Geuking MB, McCoy KD, et al. Fibroblastic reticular cells regulate intestinal inflammation via IL-15-mediated control of group 1 ILCs. *Nat Immunol.* 2016;17(12):1388-96.

48. Hayase E, Hashimoto D, Nakamura K, Noizat C, Ogasawara R, Takahashi S, Ohigashi H, Yokoi Y, Sugimoto R, Matsuoka S, et al. R-Spondin1 expands Paneth cells and prevents dysbiosis induced by graft-versus-host disease. *J Exp Med.* 2017;214(12):3507-18.

49. Takahashi S, Hashimoto D, Hayase E, Ogasawara R, Ohigashi H, Ara T, Yokoyama E, Ebata K, Matsuoka S, Hill GR, et al. Ruxolitinib protects skin stem cells and maintains skin homeostasis in murine graft-versus-host disease. *Blood.* 2018;131(18):2074-85.

50. Lantz O, Grandjean I, Matzinger P, and Di Santo JP. Gamma chain required for naive CD4+ T cell survival but not for antigen proliferation. *Nat Immunol.* 2000;1(1):54-8.

51. Valujskikh A, Lantz O, Celli S, Matzinger P, and Heeger PS. Cross-primed CD8(+) T cells mediate graft rejection via a distinct effector pathway. *Nat Immunol.* 2002;3(9):844-51.

52. Subramanian A, Tamayo P, Mootha VK, Mukherjee S, Ebert BL, Gillette MA, Paulovich A, Pomeroy SL, Golub TR, Lander ES, et al. Gene set enrichment analysis: a knowledge-based approach for interpreting genome-wide expression profiles. *Proc Natl Acad Sci U S A.* 2005;102(43):15545-50.

53. Shannon P, Markiel A, Ozier O, Baliga NS, Wang JT, Ramage D, Amin N, Schwikowski B, and Ideker T. Cytoscape: a software environment for integrated models of biomolecular interaction networks. *Genome Res.* 2003;13(11):2498-504.

54. Goold HD, Escors D, Conlan TJ, Chakraverty R, and Bennett CL. Conventional dendritic cells are required for the activation of helper-dependent CD8 T cell responses to a model antigen after cutaneous vaccination with lentiviral vectors. *Journal of immunology.* 2011;186(8):4565-72.

Author contributions

SD conceived the ideas, designed and performed experiments, analysed and interpreted data, wrote and reviewed the manuscript. PE conceived the ideas, designed and performed experiments and analysed and interpreted data. PS, TM and IRF performed experiments and analysed data. HJS and CLB provided technical and material support and reviewed the manuscript. RC conceived the ideas, supervised the study, developed methodology and wrote the manuscript.

Acknowledgements

We would like to thank Ben Seddon (University College London) for reviewing the manuscript and providing helpful feedback. This work was supported by the following research grants: S.D. (Swiss National Science Foundation, P2BSP3_158804 and P300PA_167657; European Hematology Association Fellowship and Novartis Foundation for Medical-Biological Research Fellowship); P.E. (Cancer Research UK A19503); R.C., C.L.B., S.D. and P.S. (Bloodwise, 12006); C.L.B. (Biotechnology and Biological Sciences Research Council, BB/L001608/1); C.L.B. and I.R.F. (Royal Free Charity Funding 174418). The authors have no conflicting financial interest.

Figure legends

Figure 1. Acute transcriptional response of FRC to GVHD

(A) Network visualisation of differentially up-regulated REACTOME pathways in FRC at day 7 post allo-BMT using EnrichmentMap. Enriched REACTOME pathways are depicted by red and blue nodes, where blue represents significant up-regulation in TCDBM vs. TCDBM+T and red represents significant up-regulation in TCDBM+T vs. TCDBM. **(B)** FRC populations were flow sorted from recipients with or without acute GVHD and expression of *Il-7* and *Ccl19* was analysed by quantitative RT-PCR (qPCR). Expression of the gene of interest is shown relative to the expression of the housekeeping gene *Gapdh*. **(C)** Expression of *Deaf1* in sorted FRC by qPCR. Expression of the gene of interest is shown relative to the expression of the housekeeping gene *Gapdh.* **(D)** Expression of DEAF1-dependent genes were analysed by GSEA of RNAseq data derived from FRC isolated from $GVHD^{+}$ (TCDBM, blue) versus $GVHD^{-}$ (TCDBM+T, red) recipients, from HSV-infected versus control non-infected mice, or from vaccinated mice in which FRC selectively lacked IL-17Ra versus wild type controls. Results are represented in a BubbleGUM plot in which stronger and more significant enrichments are represented by larger and darker bubbles. Blue and red colours indicate enrichment in group 1 or group 2, respectively, as indicated by the text to the left of each bubble. **(E)** Expression of known FRC-specific PTA genes relative to *Gapdh* was analysed by qPCR in sorted FRC from mice with or without GVHD by qPCR. Data represent mean±SEM. **p<0.05, Mann-Whitney U-test*

Figure 1

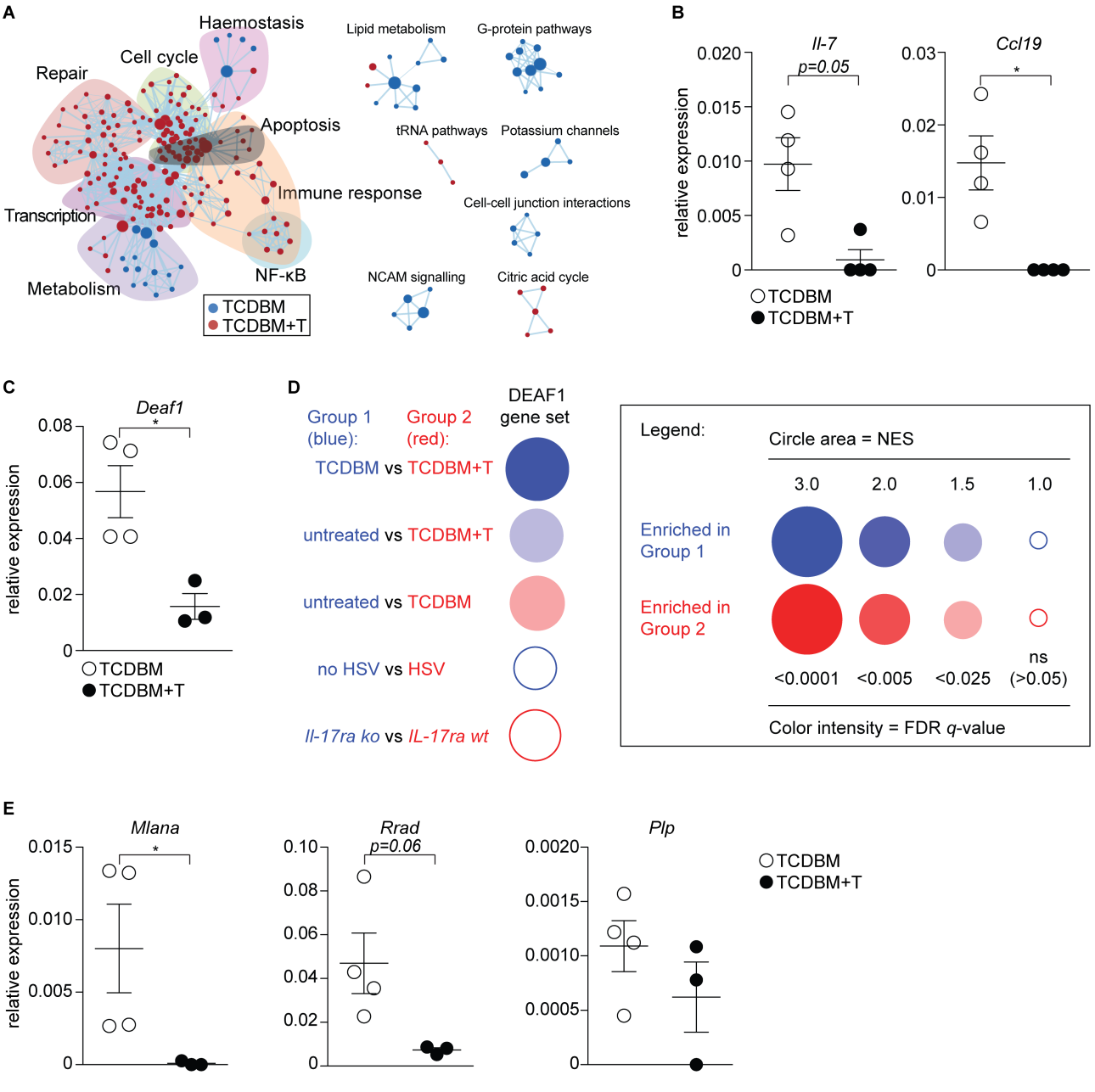
A
Haemostasis
Cell cycle
Repair
Apoptosis
Immune response
Transcription
NF-κB
Metabolism
TCDBM
TCDBM+T
Lipid metabolism
G-protein pathways
tRNA pathways
Potassium channels
Cell-cell junction interactions
NCAM signalling
Citric acid cycle
B
Il-7
p=0.05
Ccl19
*
relative expression
0.020
0.015
0.010
0.005
0
0.03
0.02
0.01
0
TCDBM
TCDBM+T
C
Deaf1
*
relative expression
0.08
0.06
0.04
0.02
0
TCDBM
TCDBM+T
D
Group 1 (blue):
Group 2 (red):
DEAF1 gene set
TCDBM vs TCDBM+T
untreated vs TCDBM+T
untreated vs TCDBM
no HSV vs HSV
Il-17ra ko vs IL-17ra wt
Legend:
Circle area = NES
3.0
2.0
1.5
1.0
Enriched in Group 1
Enriched in Group 2
<0.0001
<0.005
<0.025
ns (>0.05)
Color intensity = FDR q-value
E
Mlana
*
Rrad
p=0.06
Plp
relative expression
0.015
0.010
0.005
0
0.10
0.08
0.06
0.04
0.02
0
0.0020
0.0015
0.0010
0.0005
0
TCDBM
TCDBM+T

Figure 2. The extent and duration of FRC network injury affect its capacity for regeneration . **(A)** LN stromal cells were analysed at indicated time points after allo-BMT using the gating strategy shown. Frequencies of FRC among $CD45^-$ LN stromal cells are shown at indicated time points after BMT in TCDBM and TCDBM+T recipients. **(B)** Absolute cell numbers of LN stromal cells subsets at indicated time points after F→M BMT with either TCDBM alone or TCDBM+T. Untransplanted, age-matched mice were used as controls (data derived from 10 independent experiments). **(C)** Absolute numbers (top) and frequencies (bottom) of FRC at 3 weeks following transplantation in F→M BMT receiving Mh T cells either on day 0 (early) or 7 (late) after BMT. Dotted line indicates FRC numbers or frequencies measured in control recipients (data are representative of 3 independent experiments). **(D)** FRC frequencies and absolute numbers following 2^{nd} BMT and transfer of Mh T cells to [B6 male → *$B2m^{-/-}$* male] versus [B6 male → B6 male] BM chimeras. Plots show absolute numbers (top) and frequencies (bottom) of FRC among $CD45^-$ LN stromal cells (data are representative of 2 independent experiments). **(E)** Absolute numbers (top) and frequencies (bottom) of FRC in recipients that either received TCDBM alone or TCDBM+T with or without early anti-CD8α antibody given 2-weekly. LN stromal cells were analysed on day 28 post transplantation **(F)** Absolute numbers (top) and frequencies (bottom) of FRC in recipients that either received TCDBM alone or TCDBM+T with or without late (from day 14) anti-CD8α antibody to deplete donor CD8 T cells. LN stromal cells were analysed at indicated time points following the start of anti-CD8α treatment (data derived from 2 independent experiments). Data represent mean±SEM. **p<0.05, **p<0.01, ***p<0.001, Mann-Whitney U-test (2A+C), Kruskal-Wallis ANOVA (2B,D,E,F).*

Figure 2

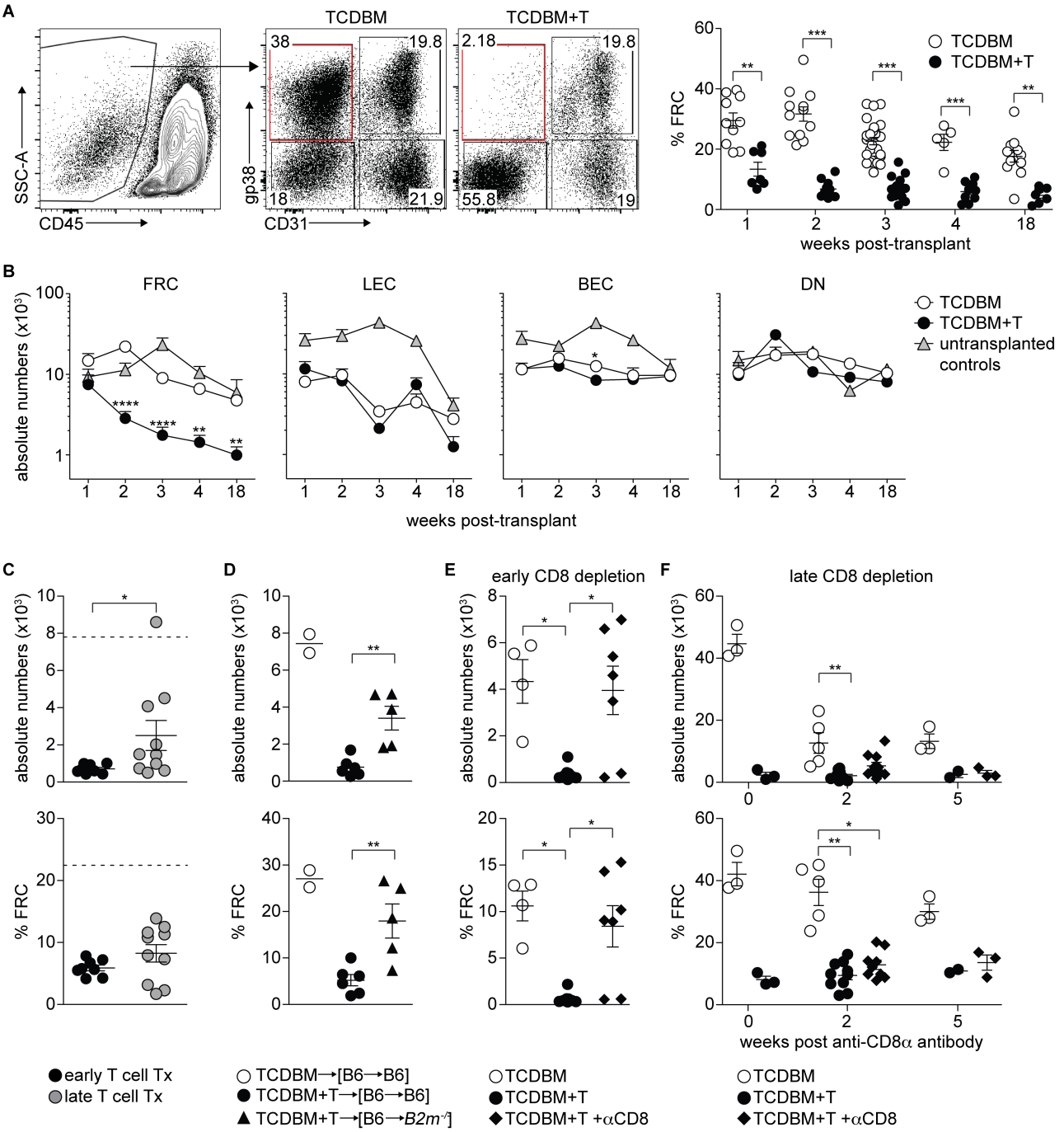
A
TCDBM
TCDBM+T
SSC-A
CD45
gp38
CD31
38
19.8
18
21.9
2.18
19.8
55.8
19
% FRC
weeks post-transplant
TCDBM
TCDBM+T
B
FRC
LEC
BEC
DN
absolute numbers (x10³)
weeks post-transplant
TCDBM
TCDBM+T
untransplanted controls
C
D
E
early CD8 depletion
F
late CD8 depletion
absolute numbers (x10³)
% FRC
weeks post anti-CD8α antibody
early T cell Tx
late T cell Tx
TCDBM→[B6→B6]
TCDBM+T→[B6→B6]
TCDBM+T→[B6→B2m⁻/⁻]
TCDBM
TCDBM+T
TCDBM+T +αCD8
TCDBM
TCDBM+T
TCDBM+T +αCD8

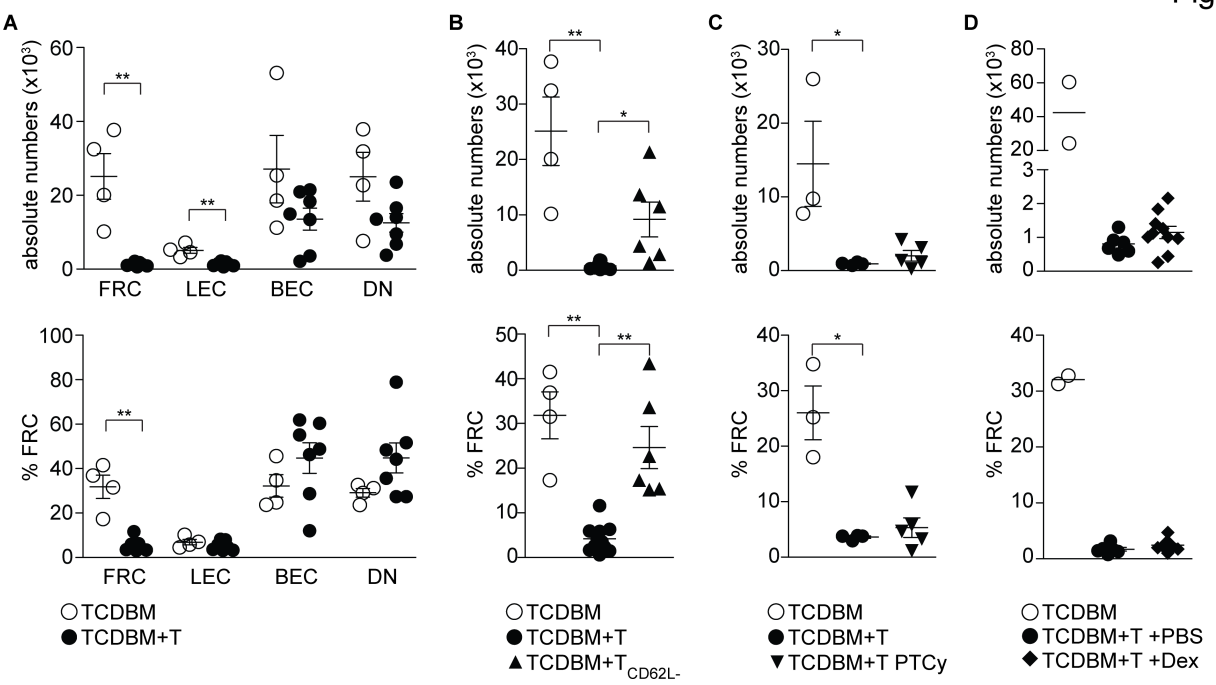

Figure 3. Effect of clinical strategies for GVHD prevention or treatment upon FRC network integrity.

(A) Absolute cell numbers (top) and frequencies (bottom) of LN stromal cell subsets in B6→129 model on day 21 post-BMT (data derived from 3 independent experiments). **(B)** Absolute FRC numbers and frequencies 21 days following BMT with either TCDBM alone, TCDBM+ polyclonal T or TCDBM+ CD62L$^-$ T cells (data derived from 4 independent experiments). **(C)** Absolute FRC numbers (top) and frequencies 18 days following BMT with either TCDBM alone or TCDBM+T with or without post-transplant cyclophosphamide (PTCy) treatment. PTCy was administered on days 3 and 4 post-transplant (25 mg/kg/day). **(D)** Absolute FRC numbers (top) and frequencies 19 days following BMT with either TCDBM alone, or TCDBM+T treated with dexamethasone (0.3 mg/kg/day) or PBS starting at day 5 after BMT (data derived from 2 independent experiments). Data represent mean±SEM. **p<0.05, **p<0.01, Mann-Whitney U-test (3A), Kruskal-Wallis ANOVA (3B+C).*

Figure 4. Acute GVHD blocks stromal re-organisation and repair of the FRC network

(A) Heatmap depicting relative expression values of specific genes involved in a stromal re-organisation programme. Relative expression is shown in FRC isolated from un-transplanted mice, or from TCDBM recipients and TCDBM+T recipients 7 days following F→M BMT. **(B)** Absolute numbers of host and donor LTi cells were evaluated at indicated time points in the presence or absence of acute GVHD following F→M BMT. Dotted line indicates mean absolute numbers of LTi cells in untreated mice (Statistical analysis of donor cells only. Data derived from 3 independent experiments). **(C)** Surface expression of VCAM1 and ICAM1 on $CD45^{-}CD31^{-}gp38^{+}$ LN stromal cells in un-transplanted controls (grey) and BMT recipients of TCDBM alone (blue) or TCDBM+T (red) at indicated time points post F→M BMT. Summary data depicting MFI of VCAM1 within the $CD45^{-}CD31^{-}gp38^{+}$ population in TCDBM or TCDBM+T recipients is shown below the respective flow cytometry plots (data derived from 6 independent experiments). **(D)** [*Rorc* wt→*Rorc* wt] or [*Rorc* ko→*Rorc* wt] chimeras were analysed for the presence of LTi cells within LN at 8 weeks after primary BMT. Plots depict expression of CD127 and RORγt among $lineage^{-}CD117^{+}$ cells. Percentage and absolute numbers of FRC is shown for [*Rorc* wt→*Rorc* wt] and [*Rorc* ko→*Rorc* wt] chimeras at 8 weeks after primary BMT (data derived from 3 independent experiments). **(E)** 8 weeks after first BMT, [*Rorc* wt→*Rorc* wt] and [*Rorc* ko→*Rorc* wt] chimeras were re-irradiated and underwent secondary F→M BMT with either TCDBM alone or TCDBM+T to induce acute GVHD. Plots show percentage (left) and absolute numbers (right) of FRC analysed at 2 weeks after the second transplantation (data derived from 2 independent experiments). Data represent mean±SEM. **p<0.05, **p<0.01, ***p<0.001, Mann-Whitney U-test (4B+C), Kruskal-Wallis ANOVA (4E).*

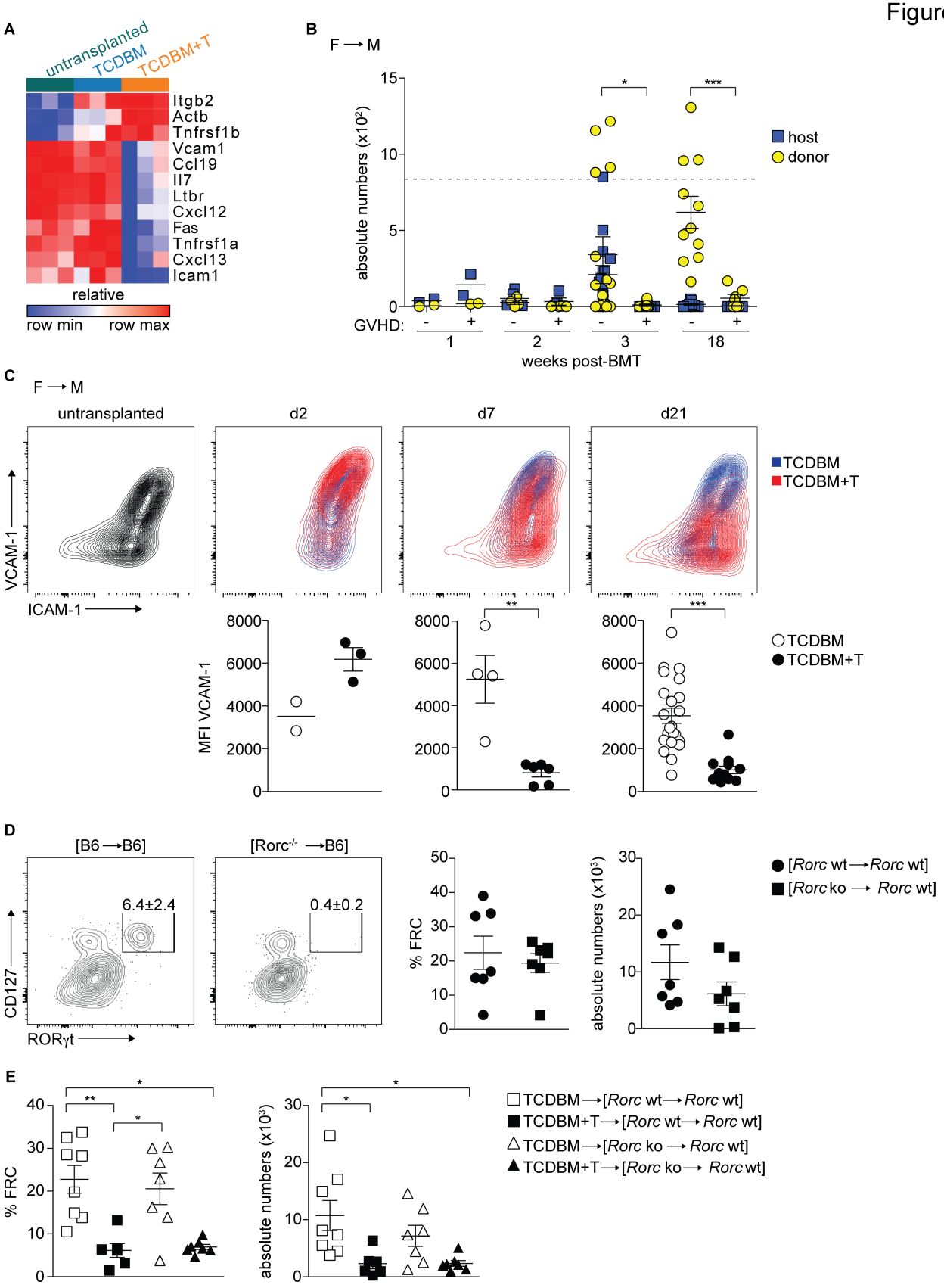
A
untransplanted
TCDBM
TCDBM+T
Itgb2
Actb
Tnfrsf1b
Vcam1
Ccl19
Il7
Ltbr
Cxcl12
Fas
Tnfrsf1a
Cxcl13
Icam1
relative
row min
row max
B
F → M
absolute numbers (x10²)
host
donor
GVHD:
weeks post-BMT
C
F → M
untransplanted
d2
d7
d21
VCAM-1
ICAM-1
TCDBM
TCDBM+T
MFI VCAM-1
D
[B6 → B6]
[Rorc-/- → B6]
6.4±2.4
0.4±0.2
CD127
RORγt
% FRC
absolute numbers (x10³)
[Rorc wt → Rorc wt]
[Rorc ko → Rorc wt]
E
% FRC
absolute numbers (x10³)
TCDBM → [Rorc wt → Rorc wt]
TCDBM+T → [Rorc wt → Rorc wt]
TCDBM → [Rorc ko → Rorc wt]
TCDBM+T → [Rorc ko → Rorc wt]

Figure 5. OVA-specific OT-I T cells fail to be purged from the periphery of iFABPtOVA mice with acute GVHD.

(A) Murine transplantation model to investigate peripheral deletion of self-reactive T cells. Acute GVHD was induced in iFABPtOVA male BMT recipients by co-transfer of female TCDBM and Mh $CD8^+$ T cells. No GVHD controls received TCDBM alone. Male B6 recipients undergoing F→M BMT with or without acute GVHD served as further controls. 6 weeks after BMT, 10^6 OT-I T cells were transferred and mice were analysed 16 days thereafter (data derived from 8 independent experiments). **(B)** Weight change in recipient mice after OT-I T cell transfer is shown as percentage of initial body weight (defined as time point of OT-I transfer). **(C)** Flow cytometry plots depict surface expression of CD45.1 and Thy1.1 among $CD8^+$ T cells (OT-I T cells are identified as $CD45.1^+Thy1.1^-$; Mh T cells are identified as $CD45.1^+Thy1.1^+$). Frequencies of OT-I T cells among total live cells in MLN and IEL are summarised in dot plots (right panel). **(D)** Absolute numbers of OT-I T cells in MLN and IEL (data derived from 7 independent experiments). **(E)** Flow cytometry plots depict intracellular IFNγ expression among $CD8^+CD45.1^+$ OT-I T cells in MLN and IEL. Percentage of $IFN\gamma^+$ OT-I T cells is summarised in dot plots (right panel). **(F)** Absolute numbers of $IFN\gamma^+$ OT-I T cells in MLN and IEL (data derived from 8 independent experiments) **(G+H)** IFNγ secretion was measured in acute $GVHD^+$ recipients in the absence or presence of donor-derived $CD11c^+$ DCs. Percentage **(G)** and absolute numbers **(H)** of $IFN\gamma^+$ OT-I T cells are shown for MLN and IEL (data derived from 3 independent experiments). Data represent mean±SEM. **p<0.05, **p<0.01, ***p<0.001, Mann-Whitney U-test (5C,D,E,F), Kruskal-Wallis ANOVA (5B,G,H).*

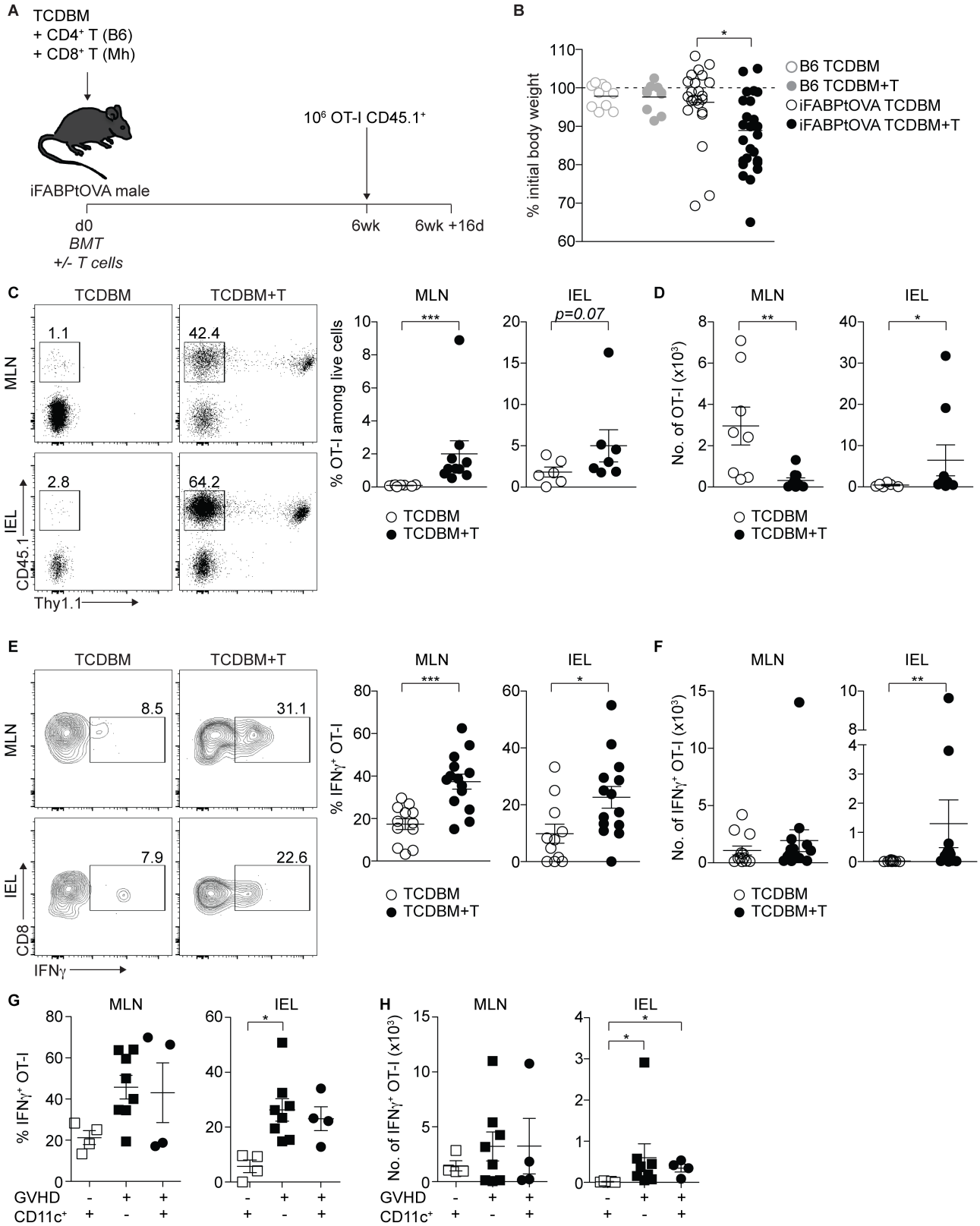
A
TCDBM
+ CD4+ T (B6)
+ CD8+ T (Mh)
iFABPtOVA male
10^6 OT-I CD45.1+
d0
BMT
+/- T cells
6wk
6wk +16d
B
% initial body weight
B6 TCDBM
B6 TCDBM+T
iFABPtOVA TCDBM
iFABPtOVA TCDBM+T
C
TCDBM
TCDBM+T
MLN
IEL
1.1
42.4
2.8
64.2
CD45.1
Thy1.1
% OT-I among live cells
p=0.07
D
No. of OT-I (x10^3)
E
8.5
31.1
7.9
22.6
CD8
IFNγ
% IFNγ+ OT-I
F
No. of IFNγ+ OT-I (x10^3)
G
H
GVHD
CD11c+

Figure 6. Specific depletion of FRC is sufficient to break peripheral tolerance of autoreactive T cells in steady state.

(A) OVA.Ccl19.DTRcre^{+} and cre^{-} mice received 500 ng DT i.p. on days -8, -6 and -4. 10^{6} OT-I T cells were transferred on day 0 and mice were analysed on day 16. **(B)** FRC depletion in OVA.Ccl19.DTRcre^{+} versus cre^{-} mice upon DT treatment. Flow cytometry plots depict surface expression of gp38 and CD31 among CD45^{-} LN stromal cells. **(C)** Weight change in OVA.Ccl19.DTRcre^{+} and cre^{-} mice is shown as percentage of initial body weight (defined as time point of OT-I transfer; data derived from 4 independent experiments). **(D)** OT-I T cells were identified as CD8^{+}CD45.1^{+}. Percentages of OT-I T cells are shown for MLN and IEL and summarised in dot plots (right). **(E)** Absolute numbers of OT-I T cells in MLN and IEL (data derived from 4 independent experiments). **(F)** IFNγ secretion measured by intracellular flow cytometry. IFNγ expression is shown among CD8^{+}CD45.1^{+} OT-I T cells. Percentage of IFNγ^{+} OT-I T cells in MLN and IEL is summarised in dot plots (right). **(G)** Absolute numbers of IFNγ^{+} OT-I T cells in MLN and IEL (data derived from 3 independent experiments). Data represent mean±SEM. **p<0.05, **p<0.01, ***p<0.001, Mann-Whitney U-test.*

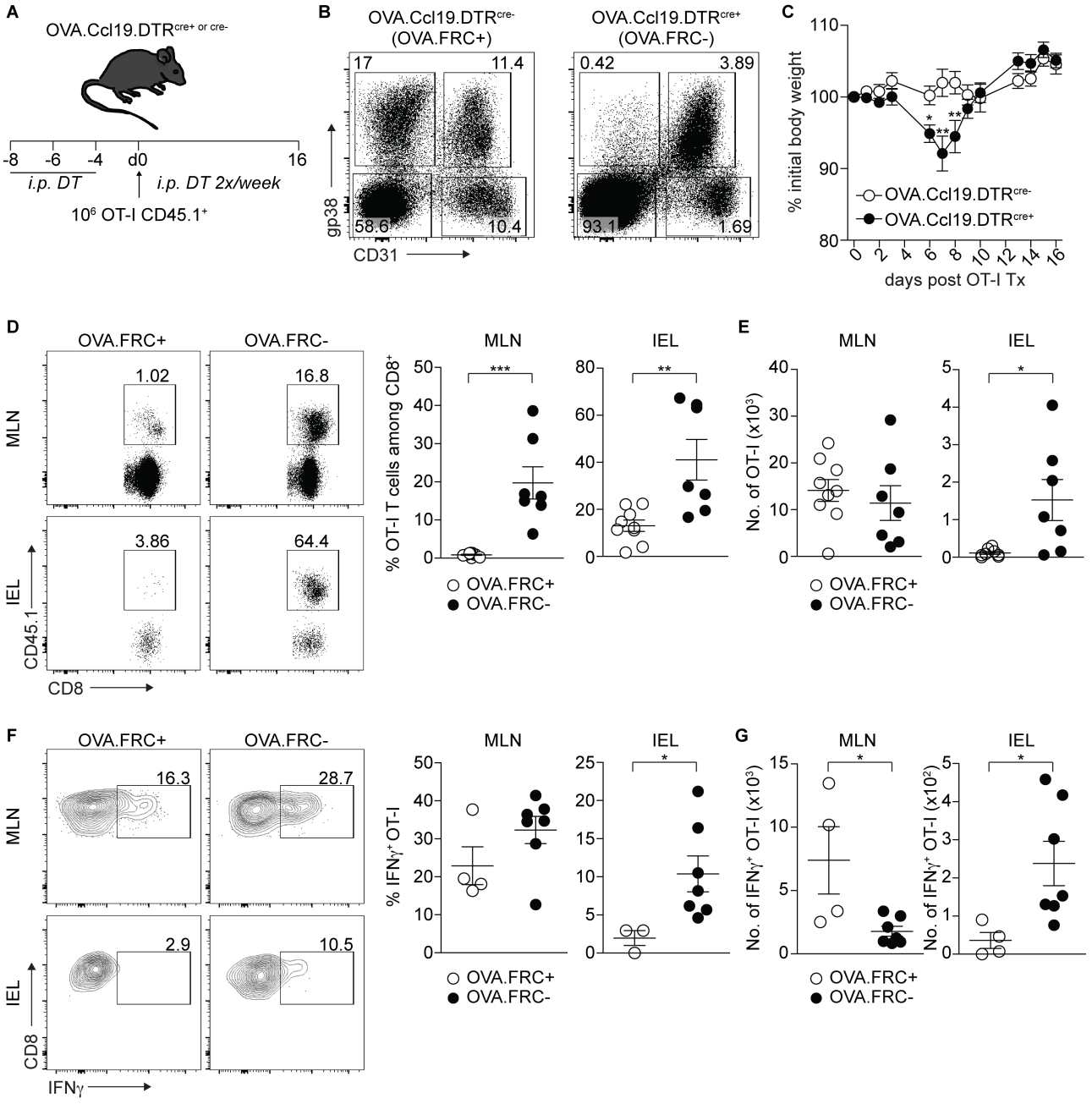
A
OVA.Ccl19.DTR cre+ or cre-
-8 -6 -4 d0 16
i.p. DT
i.p. DT 2x/week
10^6 OT-I CD45.1+
B
OVA.Ccl19.DTR cre-
(OVA.FRC+)
OVA.Ccl19.DTR cre+
(OVA.FRC-)
17
11.4
58.6
10.4
0.42
3.89
93.1
1.69
gp38
CD31
C
% initial body weight
OVA.Ccl19.DTR cre-
OVA.Ccl19.DTR cre+
days post OT-I Tx
D
OVA.FRC+
OVA.FRC-
MLN
IEL
1.02
16.8
3.86
64.4
CD45.1
CD8
% OT-I T cells among CD8+
OVA.FRC+
OVA.FRC-
E
No. of OT-I (x10^3)
F
16.3
28.7
2.9
10.5
IFNγ
% IFNγ+ OT-I
G
No. of IFNγ+ OT-I (x10^3)
No. of IFNγ+ OT-I (x10^2)

Figure 7. FRC express a distinct PTA gene signature enriched for genes normally expressed in target organs of chronic GVHD.

(A) Analytical pipeline of FRC-specific PTA candidates. **(B)** Correlation matrix of PTA candidates in published gene expression data from different LN stromal cell subsets. Pearson's correlation coefficient r between the respective subsets is indicated. FRC-enriched PTA genes are highlighted in red. The asterisk (*) symbol indicates a statistical p-value for the quality of each measured Pearson's r between any given subset, respectively; ****p<0.001* **(C)** Tissue representation of FRC-enriched PTA (≥3-fold expression compared to other LN stromal cell subsets). As control, a random set of 356 PTA, which are not enriched in FRC, was used. **(D)** Venn diagram showing the overlap between thymic PTA repressed in GVHD by >3-fold and PTA identified to be enriched in FRC compared to other LN stromal subsets. **(E)** Enrichment of the FRC-enriched PTA gene set was analysed by GSEA in FRC isolated from $GVHD^+$ versus $GVHD^-$ recipients, or from vaccinated mice in which FRC selectively lacked IL-17Rα versus wild type controls, or from HSV-infected versus control non-infected mice.

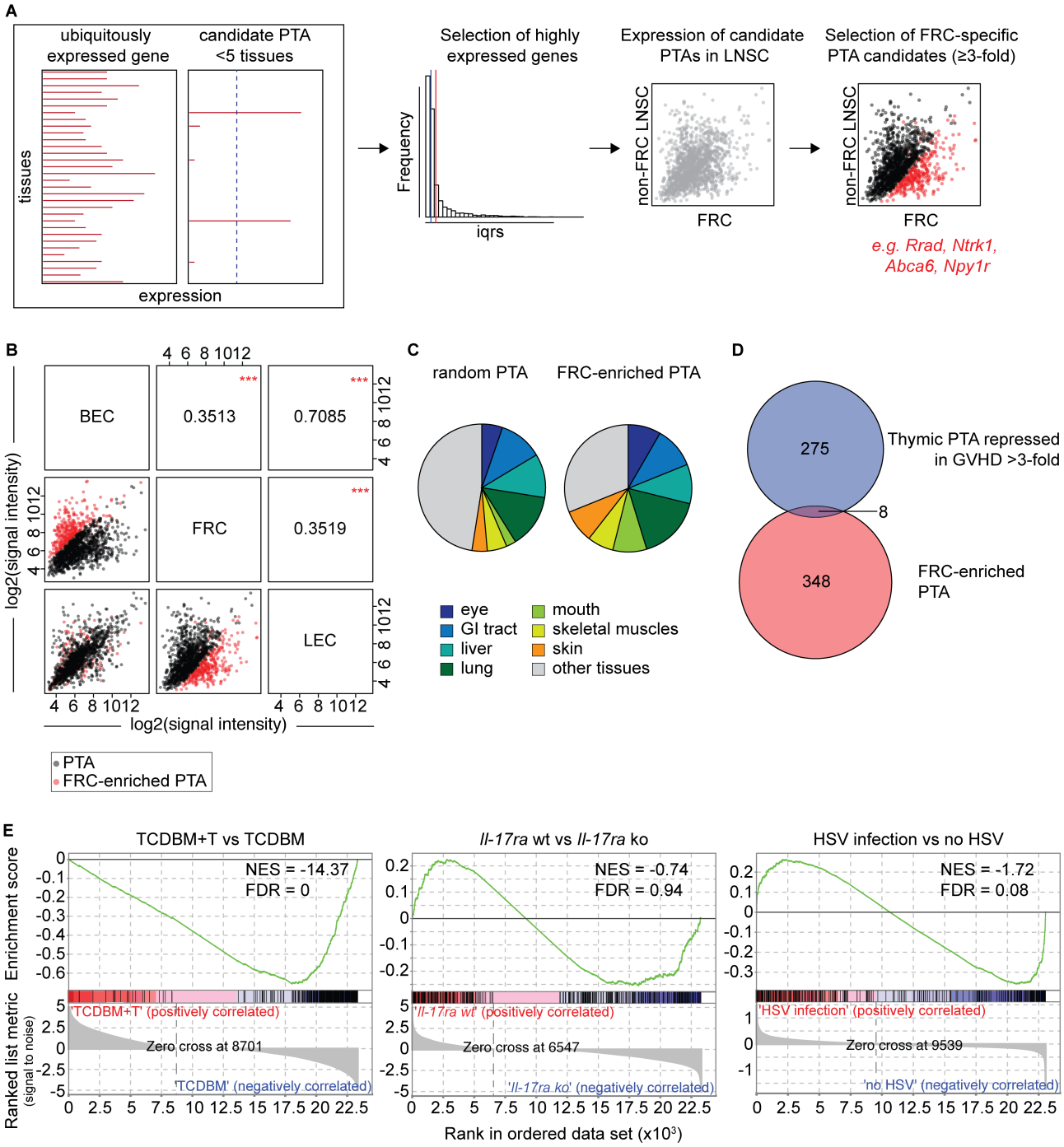
A
ubiquitously expressed gene
candidate PTA <5 tissues
tissues
expression
Selection of highly expressed genes
Frequency
iqrs
Expression of candidate PTAs in LNSC
non-FRC LNSC
FRC
Selection of FRC-specific PTA candidates (≥3-fold)
e.g. Rrad, Ntrk1, Abca6, Npy1r
B
BEC
FRC
LEC
0.3513
0.7085
0.3519
log2(signal intensity)
PTA
FRC-enriched PTA
C
random PTA
FRC-enriched PTA
eye
GI tract
liver
lung
mouth
skeletal muscles
skin
other tissues
D
275
8
348
Thymic PTA repressed in GVHD >3-fold
FRC-enriched PTA
E
TCDBM+T vs TCDBM
Il-17ra wt vs Il-17ra ko
HSV infection vs no HSV
Enrichment score
Ranked list metric (signal to noise)
NES = -14.37
FDR = 0
'TCDBM+T' (positively correlated)
Zero cross at 8701
'TCDBM' (negatively correlated)
NES = -0.74
FDR = 0.94
'Il-17ra wt' (positively correlated)
Zero cross at 6547
'Il-17ra ko' (negatively correlated)
NES = -1.72
FDR = 0.08
'HSV infection' (positively correlated)
Zero cross at 9539
'no HSV' (negatively correlated)
Rank in ordered data set (x10³)